Sensing atomic superfluid rotation beyond the standard quantum limit

Rahul Gupta [1], Pardeep Kumar [2], Rina Kanamoto [3], M. Bhattacharya [4] and Himadri Shekhar Dhar [1,5]

[1]*Department of Physics, Indian Institute of Technology Bombay, Powai, Mumbai 400076, India*
[2]*Max Planck Institute for the Science of Light, Staudtstraße 2, 91058 Erlangen, Germany*
[3]*Department of Physics, Meiji University, Kawasaki, Kanagawa 214-8571, Japan*
[4]*School of Physics and Astronomy, Rochester Institute of Technology, 84 Lomb Memorial Drive, Rochester, New York 14623, USA*
[5]*Centre of Excellence in Quantum Information, Computation, Science and Technology, Indian Institute of Technology Bombay, Mumbai 400076, India*

(Received 9 March 2024; accepted 28 October 2024; published 18 November 2024)

Atomic superfluids formed using Bose-Einstein condensates (BECs) in a ring trap are currently investigated in the context of superfluid hydrodynamics, quantum sensing, and matter-wave interferometry. The characterization of the rotational properties of such superfluids is important, but can presently only be performed by using optical absorption imaging, which completely destroys the condensate. Recent studies have proposed coupling the ring BEC to optical cavity modes carrying orbital angular momentum to make minimally destructive measurements of the condensate rotation. The sensitivity of these proposals, however, is bounded below by the standard quantum limit set by the combination of laser shot noise and radiation pressure noise. In this work we provide a theoretical framework that exploits the fact that the interaction between the scattered modes of the condensate and the light reduces to effective optomechanical equations of motion. We present a detailed theoretical analysis to demonstrate that the use of squeezed light and backaction evasion techniques allows the angular momentum of the condensate to be sensed with noise well below the standard quantum limit. Our proposal is relevant to atomtronics, quantum sensing, and quantum information.

DOI: 10.1103/PhysRevA.110.053514

I. INTRODUCTION

Quantum sensing with highly controllable ultracold atoms [1,2] is an actively developing field that provides new pathways to investigate foundational aspects of modern physics such as precise measurements of theoretically predicted fundamental constants [3,4] and ultraprecise tracking of time [5,6]. In recent years, there has been growing interest in the use of atomic superfluids such as Bose-Einstein condensates (BECs) confined inside a toroidal or ring trap for sensing [7–9]. Such configurations have been built using magnetic traps [10], time-averaged adiabatic potentials [11], painted dipole potentials [12], and intersecting "sheet" and "tube" laser beams [13]. Besides sensing, several fundamental [14–16] and technologically relevant properties have been demonstrated ranging from persistent currents [10,13] and quantum phase slips [17,18] to atomic analogs of superconducting quantum interference devices [12] and atomtronic circuits [19,20].

While investigating and harnessing the rotation of atomic superfluids are of intrinsic interest to researchers, capturing information about these rotational properties can be challenging. For instance, existing experimental approaches for probing the BEC angular momentum in ring traps completely destroy the condensate and as such do not allow for continuous observation [7,10,13,17,21,22]. Nondestructive study of (simply connected, i.e., harmonically trapped) condensates [23] captures the density profile and not the phase (or, more rigorously, the phase gradient) of the rotating states, which is necessary for estimating the angular momentum or winding number of the BECs. In fact, these methods rely on vortex precession for such measurements, which is not accessible while studying superfluids trapped in toroidal or ring traps, where the vortex is pinned, i.e., fixed in position, by the potential.

More sophisticated techniques involving ring traps involve detecting the Doppler shift in phonon modes generated in the condensate [24] or using an integrated atomic circuit, where information about the ring condensate is captured by studying the dynamics inside a tunnel-coupled rectilinear guide [25]. Recent studies [26–28] have proposed the use of quantum sensing techniques based on cavity optomechanics [29] to detect the rotational properties of superfluids in ring traps. The approach relies on the creation of sidemode excitations of the condensate due to interaction of the atoms with the orbital angular momentum (OAM) of the light [30] injected inside the cavity. While the above proposal allows for improvement in rotational sensitivity by a few orders of magnitude over other known techniques, it is still impacted by the noise imparted by the measurement setup, which restricts it to within the bounds of the standard quantum limit (SQL) [29,31].

In this work, we draw upon more powerful machinery from the toolbox of quantum optomechanics to study atomic superfluids inside a ring trap and show how to achieve rotational sensing of the condensate beyond the SQL. We consider a setup similar to that in Ref. [26], where the cavity is driven with a superposition of light beams with OAM $\pm l\hbar$, as shown in Fig. 1, thus giving rise to effective optomechanical interactions between the two sidemodes of the condensate and the optical mode. Additionally, the effect of atomic collisions

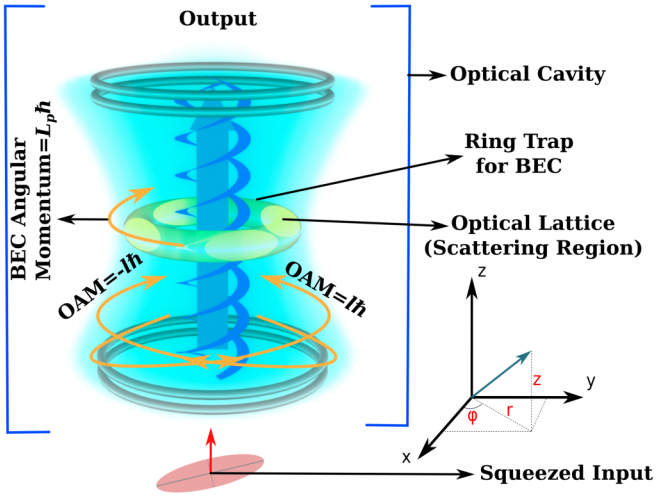

FIG. 1. BEC in a toroidal ring trap inside an optical cavity. Superposed laser beams carrying OAM $\pm\, l\hbar$ (blue corkscrew wave front and orange lines) are injected inside the cavity (blue lines). This creates an angular optical lattice (green regions) inside the ring trap (cyan toroidal shape) which contains the BEC. The input light is squeezed and shone from the bottom, while the output light after interaction is gathered from the top for homodyne detection and rotational sensing.

in the condensate is also taken into account in the system dynamics.

There are three primary active noise sources in such systems [29] that one actively seeks to mitigate. The first is the shot noise associated with light, the second is the effect of radiation pressure created by the act of measurement, which is also known as measurement backaction noise [32–34], and the third source is the thermal and quantum fluctuations of the excited modes of the condensate. Using phase-squeezed light as input [35,36], the noise can be significantly lowered, especially at low input powers where the shot noise is dominant, thus achieving significantly higher sensitivity in detecting rotational properties of BECs in a toroidal trap. However, using squeezed light alone is not sufficient to overcome the radiation pressure or backaction noise, which prevents the noise spectrum from going below the SQL. To overcome this, sophisticated quantum nondemolition measurement techniques are often required [37–44], which can mitigate the effect of measurement backaction. In this work, we consider a quantum nondemolition method based on backaction evasion (BAE) measurements in a hybrid system [45,46], consisting of the two BEC sidemodes and the optical cavity field.

For the condensate in a ring trap, the BAE measurement approach is based on driving the cavity with two off-resonant optical fields [47]. The key idea here is for the cavity mode to couple dynamically to only one pair of collective quadratures of the two condensate modes, which are then measured. However, the measurement backaction only drives the conjugate set of quadratures, which do not affect the dynamics. Going beyond the conventional analysis [47], we adopt a Floquet-theory-based approach to obtain the steady states of an optomechanical system using a bichromatic drive. However, unlike the previous studies [48–50], we consider a hybrid system consisting of two sidemodes of the condensate and the optical cavity and extend the formalism to work in the bad cavity regime. The time-dependent equations of motion are solved beyond the rotating-wave approximation, where counterrotating terms are present. Using such a BAE method, we find that nondemolition measurements of the scattered modes can be performed with the noise spectrum going below the SQL. Importantly, we show that by combining the BAE scheme with phase-squeezed input light [51] in the cavity, the angular momentum of the condensate can be measured with high sensitivity and noise below the SQL even at higher input powers.

The paper is arranged as follows. In Sec. II, the physical setup of a BEC confined in a toroidal trap, placed inside a cavity, is presented. This is followed by Sec. III, where the theoretical framework for rotational sensing using squeezed OAM-carrying modes is presented. In Sec. IV, the backaction evasion method using a bichromatic driving field is introduced in the context of rotational sensing, with derivation of the equations of motion beyond the rotating-wave approximation. A summary and conclusions are presented in Sec. V.

II. MODEL

The primary setup consists of a BEC or an atomic superfluid of N atoms, each of mass m, confined in a ring trap [10–13], which is then placed at the center of an optical cavity, as shown in Fig. 1. The condensate is trapped using an axial harmonic potential $\frac{1}{2}m\omega_z z^2$ in the vertical z direction and an annular ring trap with radius R in the x-y plane, with the radial potential $\frac{1}{2}m\omega_r(r-R)^2$. For such a trap, the dynamics of the condensate can be limited to a single dimension, i.e., the unhindered azimuthal motion in the φ direction of the ring trap [26,52].

For sensing the BEC rotation, a laser beam of frequency ω is diffracted and recombined to form a superposed pair of beams with optical angular momenta $\pm l\hbar$ [53]. The cavity with resonant frequency ω_a and containing the trapped BEC is then coherently driven by these OAM beams. Importantly, such a driving leads to the formation of an optical lattice around the axis of the cavity in the azimuthal direction (see Fig. 1). If the condensate rotating inside the cavity has a winding number L_p, a small number of atoms will experience first-order Bragg scattering from the optical lattice [54] and attain the final winding numbers $L_\pm = L_p \pm 2l$, respectively. For a weak lattice [26], the number of atoms undergoing higher-order scattering will be negligible compared to the number of atoms contained in the zeroth (unscattered) and first-order scattering sidemodes. We note that even the first-order scattered sidemodes contain a very small fraction of the total number of atoms in the condensate. As such, the sidemodes have a negligible chemical potential and the temperature is not significantly affected due to scattering. This is in contrast to cases where splitting of the BEC occurs to form new condensed modes [55].

The condensate is represented by atomic operators $\Phi(\varphi)$, where the angle φ is the azimuthal degree of freedom. Following the scattering picture presented above, the atomic operator can be represented in terms of the persistent current (C) and the first-order sidemodes ($C_\pm$) such that

$$\Phi(\varphi) = \frac{e^{iL_p\varphi}}{\sqrt{2\pi}}C + \frac{e^{iL_+\varphi}}{\sqrt{2\pi}}C_+ + \frac{e^{iL_-\varphi}}{\sqrt{2\pi}}C_-, \tag{1}$$

where the total number of atoms in terms of the bosonic operators is $C^\dagger C + C_+^\dagger C_+ + C_-^\dagger C_- = N$. Assuming that the sidemodes are sparsely occupied and taking a mean-field approximation for the macroscopic C mode such that $C^\dagger C \approx C^* C = N$, one can define the operators $c = C^* C_+/\sqrt{N}$ and $d = C^* C_-/\sqrt{N}$. The Hamiltonian of the system, using the above operators and written in the frame rotating with the driving frequency, reduces to [26]

$$H/\hbar = \Delta a^\dagger a + \omega_c c^\dagger c + \omega_d d^\dagger d + G a^\dagger a (X_c + X_d) - i\eta(a - a^\dagger) + g\mathcal{Z}, \tag{2}$$

where $\omega_{c\,(d)} = (L_p \pm 2l)^2\hbar/2I$ (I is the moment of inertia of each atom about the center of the ring) and $a^\dagger$ and a are the creation and annihilation operators, respectively, of the optical cavity field. The term Δ denotes the effective detuning between the driving and cavity frequency. The field injected in the cavity is a single-mode superposition of frequency degenerate OAM light $|+l\hbar\rangle + e^{i\varphi_0}|-l\hbar\rangle$, where the relative phase φ_0 can be fixed by the experimentalist. The light intensity in the corresponding optical lattice varies as $\cos^2(l\varphi - \varphi_0/2)$, where φ is the azimuthal degree of freedom. The scattering with atoms in the BEC only transforms $|\pm l\hbar\rangle \to |\mp l\hbar\rangle$, and the optical lattice remains unchanged. This implies no new optical modes are populated. In this work we consider $\varphi_0 = 0$, which gives us a symmetric superposition of $|\pm l\hbar\rangle$ (see Appendix A for further details). The displacement operators of the atomic sidemodes are given by $X_c = (c + c^\dagger)/\sqrt{2}$ and $X_d = (d + d^\dagger)/\sqrt{2}$, where the effective optomechanical interaction between the displacement $X_{c\,(d)}$ and the optical lattice is given by G. In addition, η is the driving amplitude of the input beam. The final term $g\mathcal{Z}$ represents the effect of collisions between atoms in the BEC, where g is the interaction between any two atoms. The term G and operator $\mathcal{Z}$ are derived in Ref. [26], with $G = g_a^2\sqrt{N}/2\sqrt{2}\Delta_a$, where g_a is the coupling strength of a photon with a single atom and Δ_a is the detuning of the input beam with the atomic transition level; $\mathcal{Z}$ contains collision operators up to order N, which significantly contributes to the dynamics.

III. ROTATIONAL SENSING USING SQUEEZED LIGHT

The few-mode effective Hamiltonian in Eq. (2) describes the system consisting of the condensate with a winding number L_p and interacting with the optical field carrying OAM $\pm l\hbar$. The dynamics of the system can be written in the form of the quantum Langevin equations [29,56]. They can be obtained by writing the Heisenberg equations of motion for the cavity and the sidemode operators. Below we express the equations in terms of only the cavity and position quadrature of sidemodes, which resemble a pair of damped oscillators, driven by photons and stochastic noise operators,

$$\ddot{X}_c + \gamma\dot{X}_c + \Omega_c^2 X_c = -\tilde{\omega}_c G a^\dagger a - \mathcal{A}X_d + \omega_c \epsilon_{c,\mathrm{in}}, \tag{3}$$

$$\ddot{X}_d + \gamma\dot{X}_d + \Omega_d^2 X_d = -\tilde{\omega}_d G a^\dagger a + \mathcal{A}X_c + \omega_d \epsilon_{d,\mathrm{in}}, \tag{4}$$

$$\dot{a} = \{i[\Delta - G(X_c + X_d)] - \kappa/2\}a + \eta + \sqrt{\kappa}a_{\mathrm{in}}, \tag{5}$$

where $\Omega_{c\,(d)}^2 = (\omega_{c\,(d)} + 4gN)^2 - 4g^2N^2$ and $\mathcal{A} = 2gN(\omega_c - \omega_d)$ are the modified sidemode frequencies and coupling between them, respectively. The contributions from the interatomic collisions with strength g arise from the operator $\mathcal{Z}$ in Eq. (2) [26]. The damping and cavity loss rates are given by γ and κ, respectively, and the shifted frequencies $\tilde{\omega}_{c\,(d)} = \omega_{c\,(d)} + 2gN$. The driving term $\eta = \sqrt{\mathcal{P}_{\mathrm{in}}\kappa/\hbar\omega_a}$, where $\mathcal{P}_{\mathrm{in}}$ is the input laser power and $\epsilon_{c\,(d),\mathrm{in}}$ and a_{in} are the input noise operators that take into account the thermal and quantum noise in the atomic sidemodes and the cavity modes, respectively.

In the Langevin formalism [29,56], the noise enters the equations in the form of correlation functions, where the mean fluctuations are zero, i.e., $\langle\epsilon_{c\,(d),\mathrm{in}}\rangle = \langle a_{\mathrm{in}}\rangle = 0$. We introduce squeezing in the optical modes using the input-output formalism, which allows for modeling quantum fluctuations injected into the cavity, in addition to any laser-driven coherent state. As such, squeezed vacuum fluctuations a_{in} are added on top of the coherent cavity state a, which can be experimentally realized using a combination of beam splitters and an optical parametric oscillator [57,58]. Now if the input cavity mode is squeezed, the general correlations of the noise operators are given by [29,36],

$$\begin{aligned}
\langle Q_{\mathrm{in}}(\omega)Q_{\mathrm{in}}(\omega')\rangle &= (2N_r + 1 + M_r + M_r^*)\pi\delta(\omega + \omega'),\\
\langle P_{\mathrm{in}}(\omega)P_{\mathrm{in}}(\omega')\rangle &= [2N_r + 1 - (M_r + M_r^*)]\pi\delta(\omega + \omega'),\\
\langle Q_{\mathrm{in}}(\omega)P_{\mathrm{in}}(\omega')\rangle &= i[1 + (M_r^* - M_r)]\pi\delta(\omega + \omega'),\\
\langle P_{\mathrm{in}}(\omega)Q_{\mathrm{in}}(\omega')\rangle &= i[-1 + (M_r^* - M_r)]\pi\delta(\omega + \omega'),\\
\langle \epsilon_{k,\mathrm{in}}(\omega)\epsilon_{k,\mathrm{in}}(\omega')\rangle &= \mathcal{B}_k\left[\coth\left(\frac{\hbar\omega_k}{2k_BT_k}\right) + 1\right]\delta(\omega + \omega'),
\end{aligned} \tag{6}$$

where $Q_{\mathrm{in}} = (a_{\mathrm{in}} + a_{\mathrm{in}}^\dagger)/\sqrt{2}$ and $P_{\mathrm{in}} = i(a_{\mathrm{in}}^\dagger - a_{\mathrm{in}})/\sqrt{2}$ are the quadrature operators of the incident light. Here $\mathcal{B}_k = 2\pi\gamma\omega/\omega_k$ and T_k is the temperature of the BEC, where $k = \{c, d\}$. The N_r and M_r are related to squeezing parameters r and θ and are given by

$$N_r = \sinh^2 r + N_a(\omega_a)(\sinh^2 r + \cosh^2 r), \tag{7}$$

$$M_r = e^{i\theta}\sinh r\cosh r[2N_a(\omega_a) + 1], \tag{8}$$

where $N_a(\omega_a)$ is the number of thermal photons, which we have neglected as the cavity frequency is in the optical regime. Moreover, in the absence of squeezing, the terms N_r and M_r are identically zero, and the optical noise correlations reduce to $\langle a_{\mathrm{in}}(\omega)a_{\mathrm{in}}^\dagger(\omega')\rangle = 2\pi\delta(\omega + \omega')$.

For sensing the winding number L_p of the BEC inside the ring trap, the central idea is to detect the phase quadrature of the cavity output field, which contains the two frequencies Ω_c and Ω_d [26]. A heuristic reading of Eqs. (3) and (4) in the absence of any noise and negligible radiation pressure shows that the sideband mode displacements X_c and X_d oscillate at frequencies Ω_c and Ω_d, which in turn governs the optical field in Eq. (5), as the field operator a is coupled to the two sideband modes. A homodyne detection of the output

optical phase quadrature $P_{\rm out}(\omega)$ should therefore give a spectral density $S(\omega)$, which peaks at Ω_c and Ω_d. Now if $4g^2N^2 \ll (\omega_{c\,(d)} + 4gN)^2$, the spectral peaks are given by $\Omega_{c\,(d)} \approx \omega_{c\,(d)} + \Delta\omega_{\rm coll}$, where $\Delta\omega_{\rm coll} = 2gN(2 - gN/\omega_{c(d)})$. As such, by measuring the gap between the spectral peaks $\Omega_c - \Omega_d = \omega_c - \omega_d = 4L_p l\hbar/I$, where l and I are already known, and the winding number L_p of the BEC can be estimated. The objective now is to find the optimal conditions such that measurement of the output spectrum can be performed with minimal noise and high sensitivity. To achieve this, the equations of motion need to be solved to obtain the spectral density of the output optical field.

The steady-state solutions of Eqs. (3)–(5) are given by $X^s_{c\,(d)} = -\tilde{\omega}_{c\,(d)} G|a^s|^2/\Omega^2_{c\,(d)} - \mathcal{A}X^s_{d\,(c)}$ and $a^s = -\eta/\alpha$, where $\alpha = i[\Delta - G(X^s_c + X^s_d)] - \kappa/2$. These solutions exhibit bistability, and for studying the spectral distribution and noise sensitivity, it is preferable to work in the monostable regime [26]. A linear-response analysis can then be performed around monostable steady states such that the system operators can be written as $K = K^s + \delta K$, where $K = \{a, X_c, X_d\}$. Moreover, the analysis can be carried out in the frequency domain by taking Fourier transforms. Linearizing around the steady state, the relations in Eqs. (3)–(5) can be rewritten in frequency space as $\mathcal{F}\delta u = D u_{\rm in}$, where the matrix $\mathcal{F}$ is given by

$$\mathcal{F} = \begin{pmatrix} \chi_a^{-1} & \Delta' & 0 & 0 \\ -\Delta' & \chi_a^{-1} & \sqrt{2}Ga_s & \sqrt{2}Ga_s \\ \sqrt{2}Ga_s\tilde{\omega}_c & 0 & \chi_c^{-1} & \mathcal{A} \\ \sqrt{2}Ga_s\tilde{\omega}_d & 0 & -\mathcal{A} & \chi_d^{-1} \end{pmatrix}, \tag{9}$$

$\delta u = [\delta Q, \delta P, \delta X_c, \delta X_d]^T$ and $u_{\rm in} = [Q_{\rm in}, P_{\rm in}, \epsilon_{c,{\rm in}}, \epsilon_{d,{\rm in}}]^T$ are vectors containing the fluctuation and input noise operators, respectively, such that $\delta Q = (\delta a + \delta a^\dagger)/\sqrt{2}$ and $\delta P = i(\delta a^\dagger - \delta a)/\sqrt{2}$, and $D = {\rm diag}[\sqrt{\kappa}, \sqrt{\kappa}, \omega_c, \omega_d]$ is a diagonal matrix with the system loss rates as elements. In addition, $\chi_a^{-1}(\omega) = \kappa/2 - i\omega$ and $\chi_{c\,(d)}^{-1}(\omega) = \Omega^2_{c\,(d)} - i\omega\gamma - \omega^2$ are susceptibility functions. The above matrix equation can be inverted to obtain the required analytic and numerical solutions for $\delta P(\omega)$ and $\delta Q(\omega)$. Now using the input-output formalism [46,59], the output optical quadrature can be found from the relation $\delta K_{\rm out}(\omega) = \sqrt{\kappa}\delta K(\omega) - \delta K_{\rm in}(\omega)$ for $K = \{Q, P\}$. Note that the prefix δ in front of input and output terms is dropped henceforth, for compactness. The analytical expressions for these coefficients are provided in Appendix B.

To obtain the noise spectral density of the output quadrature, one needs to cause the interference of the cavity output with a local oscillator to perform homodyne detection. The injected laser itself can serve as the local oscillator which is combined with the output signal. This allows for the extraction of the phase-rotated optical quadrature where the rotation angle ϕ can be tuned by adjusting a constant phase shift between the two signals. We define a generalized quadrature $Q^\phi_{\rm out}(\omega)$ at ϕ and its spectral density $S^{\rm out}_{Q^\phi,Q^\phi}(\omega)$ as

$$Q^\phi_{\rm out}(\omega) = Q_{\rm out}(\omega)\cos\phi + P_{\rm out}(\omega)\sin\phi, \tag{10}$$

$$S^{\rm out}_{Q^\phi,Q^\phi}(\omega) = \frac{1}{2\pi}\int_{-\infty}^{\infty} d\omega' \langle Q^\phi_{\rm out}(\omega) Q^\phi_{\rm out}(\omega')\rangle. \tag{11}$$

By varying the spectral density over different phase angles, we note that $\phi = \pi/2$ is optimal for maximum detection for an unsqueezed input beam, i.e., $Q^\phi_{\rm out}(\omega) = P_{\rm out}(\omega)$. The optimal spectral density is then given by

$$\begin{aligned} S^{\rm out}_{P,P}(\omega) &= A_P A_P \chi_{QQ} + B_P B_P \chi_{PP} + A_P B_P \chi_{QP} \\ &\quad + B_P A_P \chi_{PQ} + C_P C_P \chi_{CC} + D_P D_P \chi_{DD}, \\ \chi_{XY} &= \frac{1}{2\pi}\int_{-\infty}^{\infty} d\omega' \langle X_{\rm in}(\omega) Y_{\rm in}(\omega')\rangle, \end{aligned} \tag{12}$$

where $X_{\rm in}, Y_{\rm in} \in \{Q_{\rm in}, P_{\rm in}, \epsilon_c, \epsilon_d\}$. The calculations for the detection angle ϕ that optimize the noise spectrum and sensitivity under different conditions are provided in Appendix C.

The second important figure of merit is the sensitivity with which the spectral density and therefore the rotational properties of the BEC can be measured. This is defined as [26,60]

$$\zeta(\omega) = \frac{S(\omega)}{\partial S(\omega)/\partial\Lambda}\sqrt{t_{\rm meas}}, \quad \zeta_{\rm opt} = \zeta(\omega = \omega_{\rm opt}), \tag{13}$$

where $t_{\rm meas} \approx \kappa/8a_s^2G^2$ is the measurement time in the bad cavity regime [29] and $\omega_{\rm opt}$ satisfies $(\frac{\partial\zeta}{\partial\omega})_{\omega=\omega_{\rm opt}} = 0$. The optimal sensitivity $\zeta_{\rm opt}$ corresponds to the minima of the function $\zeta(\omega)$ at frequency $\omega_{\rm opt}$. The motive here is to find an optimal frequency where the change in the spectrum $S(\omega)$ is maximum, which is often relevant in experimental implementations using a lock-in detection scheme [60]. Moreover, $S(\omega)$ responds linearly with angular momentum $\Lambda = L_p\hbar$ at values of L_p relevant to our analysis such that $S(\omega)(\frac{\Delta S(\omega)}{\Delta\Lambda})^{-1} \simeq S(\omega)(\frac{\partial S(\omega)}{\partial\Lambda})^{-1}$, which is useful for numerical estimation of sensitivity.

Figure 2 shows the variation of $S^{\rm out}_{P,P}(\omega)$ and $\zeta(\omega)$ with frequency ω and studies the effect of introducing squeezed input and atomic collisions in the condensate by solving Eqs. (3)–(5). The winding number of the input light and the BEC are taken as $l = 10$ and $L_p = 1$, respectively, which results in peaks of the output spectrum at $\Omega_{c\,(d)}/2\pi$ at 569 and 695 Hz, respectively, without collisions and 624 and 750 Hz, respectively, with collisions, when $gN = 14$ Hz. The optimal sensitivity $\zeta_{\rm opt}$ also occurs at $\omega_{\rm opt} \approx \Omega_{c\,(d)}$. The plots in Fig. 2 show that the presence of interatomic interactions g simply shifts the frequencies of the spectral peaks and also the optimal sensitivity for both squeezed and unsqueezed light (cf. [26]). However, for squeezed light with amplitude $r = 2$ and angle $\theta = \pi$, the spectral density drops below the shot-noise level, which indicates that the noise in the spectrum can be lowered below the quantum limit. For detection angle $\phi = \pi/2$ and squeezing angle $\theta = \pi$, the optimal sensitivity $\zeta_{\rm opt}$ of the measurement is not significantly enhanced over the unsqueezed case.

To better understand the enhancement of measurement sensitivity with squeezing, we look at Fig. 3, which shows the variation of the factor $\zeta_{\rm opt}(0,0)/\zeta_{\rm opt}(r,\theta)$ with the squeezing amplitude r and angle θ. For enhancement, the sensitivity with squeezing should be lower compared to the unsqueezed case and therefore the factor should be greater than unity. Notably, $\zeta_{\rm opt}(0,0)/\zeta_{\rm opt}(r,\theta) \geqslant 1$ for all values of r. The best enhancement for input power $\mathcal{P}_{\rm in} = 12.4$ fW is observed for angles $\theta = \{2\pi/3, 4\pi/3\}$ where a factor of 2 (3 dB) can be achieved,

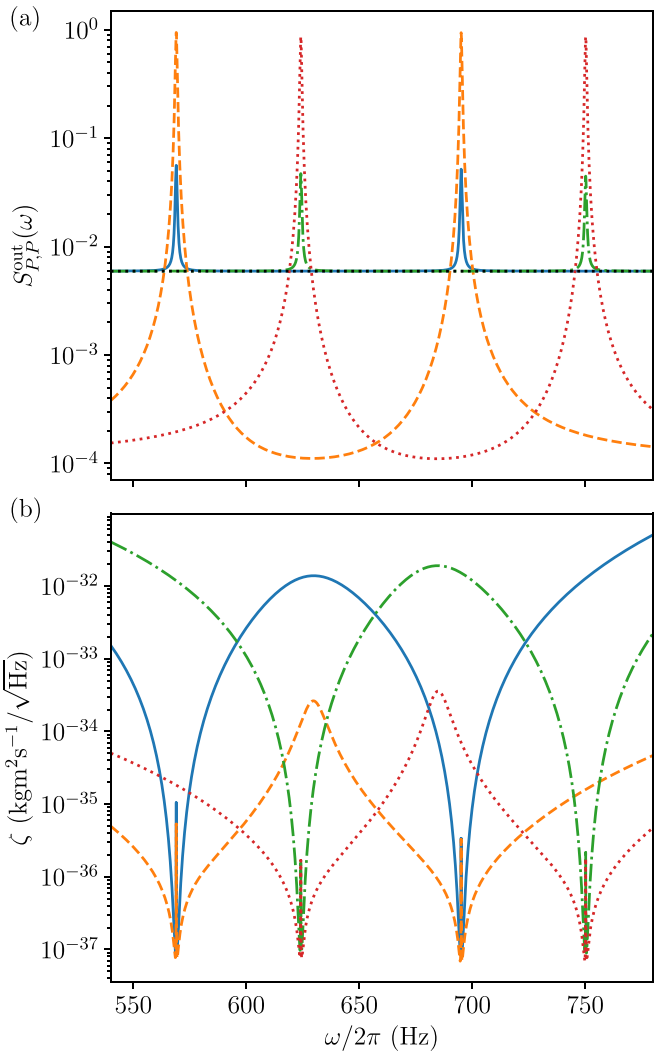

FIG. 2. Variation of spectral density and sensitivity with frequency. (a) Output optical noise spectral density for unsqueezed ($r = 0$, blue solid line) and squeezed ($r = 2$ and $\theta = \pi$, orange dashed line) input, without interatomic collisions ($g = 0$). Cases with interatomic interactions ($g \neq 0$) are indicated with a green dash-dotted line for $r = 0$ and with a red dotted curve for $r = 2$ and $\theta = \pi$. For squeezing angle $\theta = \pi$, the noise spectrum falls below the shot-noise level (black dotted horizontal line). (b) Variation of sensitivity for the same set of parameters as in (a). The input power $\mathcal{P}_{\rm in} = 12.4$ fW and the detection angle $\phi = \pi/2$. The parameters $N = 10^4$, $R = 12$ μm, $gN \approx 14$ Hz, $I/\hbar = 0.0505$ Hz, and $G/2\pi = 7.5$ kHz, correspond primarily to a condensate of sodium atoms [26]. The other parameters are $\omega_a/2\pi = 10^3$ THz, $\omega_r/2\pi = \omega_z/2\pi = 42$ Hz, $\kappa/2\pi = 2$ MHz, $\gamma/2\pi = 0.8$ Hz, $\Delta' = 0$, $T_{c,d} = 20$ nK, $l = 10$, and $L_p = 1$.

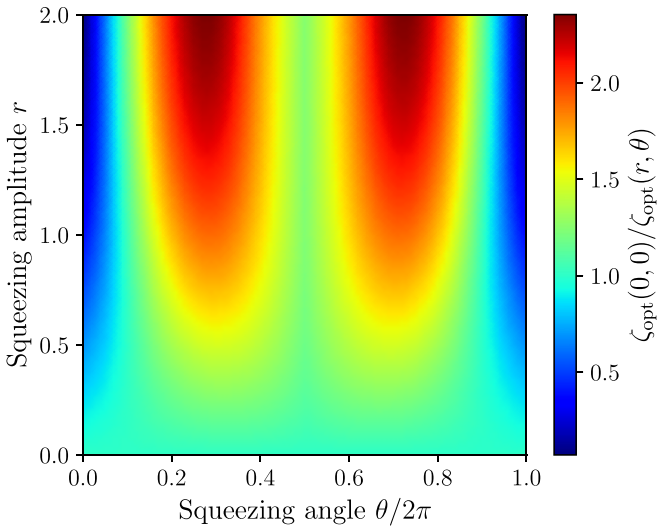

FIG. 3. Variation of the sensitivity enhancement factor between unsqueezed and squeezed input, as a function of the squeezing amplitude r and angle θ. Here $\mathcal{P}_{\rm in} = 12.4$ fW. All the other parameters are the same as in Fig. 2.

which saturates for $r > 2$. For $\theta = \pi$, the enhancement factor is close to unity and the sensitivity for squeezed light is similar to those achieved using unsqueezed light, as seen in Fig. 2. However, the enhancement with squeezing can be much larger at lower values of $\mathcal{P}_{\rm in}$, up to a saturation value around 18 dB.

The optical spectral density $S^{\rm out}_{P,P}(\omega)$ is given by

$$S^{\rm out}_{P,P}(\omega) = S_{\rm sn} + S_{\rm rp} + S_{\rm th} + S_{\rm add},$$

where

$$S_{\rm sn} = B_P(\omega)B_P(-\omega)\frac{\chi_{PP}}{2}, \tag{14}$$

$$S_{\rm th} = C_P(\omega)C_P(-\omega)\chi_{CC} + D_P(\omega)D_P(-\omega)\chi_{DD}, \tag{15}$$

$$S_{\rm rp} = \text{all terms of } O(G^2). \tag{16}$$

Note that the spectrum is normalized and the additional term $S_{\rm add}$ is present only for squeezed input. Figure 4 shows the variation of the spectral density $S^{\rm out}_{P,P}(\omega)$ with input power $\mathcal{P}_{\rm in}$, at the optimal frequency $\omega = \omega_{\rm opt}$. The figure also shows the contribution due to optical shot noise $S_{\rm sn}$ and radiation pressure $S_{\rm rp}$ (blue and orange solid lines, respectively). In the absence of squeezing, the minimum of $S^{\rm out}_{P,P}(\omega)$ at temperature $T_{c,d} = 20$ nK and frequency $\omega_{\rm opt}$ gives us the minimum noise $S_{\rm min}$. This is achieved at optimal input power $\mathcal{P}^{\rm out}_{\rm in}$, as shown in Fig. 4 (black solid curve). Now if $T_{c,d} = 0$, the noise $S_{\rm th}$ can be further lowered to ultimately achieve the standard quantum limit $S_{\rm SQL}$. Using squeezed input, with amplitude $r = 2$ and $\theta = \pi$, the output spectral density $S^{\rm out}_{P,P}$ can be lowered significantly below the minimum noise, thus providing a clear advantage over unsqueezed light for lower values of $\mathcal{P}_{\rm in}$. However, the minimal noise spectral density can only get close to SQL but not below it, regardless of the value of r or θ. In fact, for $\theta = 0$, the noise is higher than the minimum noise. This is primarily due to the measurement backaction noise becoming significant at higher powers. As such, using squeezing alone in the input optical light with OAM, the noise cannot be lowered beyond the SQL. To break the SQL one needs to counter the backaction noise using quantum nondemolition measurement [37,38], which can be achieved with or without using squeezed light [39].

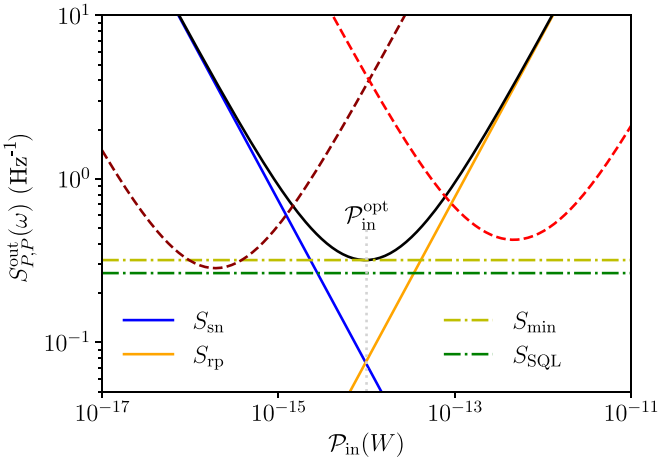

FIG. 4. Change in optimal output spectrum density at $\omega_{\rm opt}$ with input power. The output spectrum density (black solid line) is minimum at an optimal power $\mathcal{P}^{\rm opt}_{\rm in}$, where the decreasing shot noise (blue solid line) and increasing radiation pressure (orange solid line) intersect. The spectrum density with squeezed input (brown dashed line) with $r = 2$ breaks the minimum noise $S_{\rm min}$ (light green dash-dotted line) at squeezing angle $\theta = \pi$ at lower input powers. For $\theta = 0$, the spectrum density remains above this minimum noise. The spectrum density remains above the standard quantum limit $S_{\rm SQL}$ (dark green dash-dotted line) for all squeezing values and input power. The other parameters are the same as in Fig. 2.

IV. ROTATIONAL SENSING USING BACKACTION EVASION

The measurement of a quantum system typically involves its interaction with an additional detection or measuring device. During the measurement of an observable $\hat{X}$ of the system, system-detector interactions can introduce noise in the system via the variable conjugate to $\hat{X}$, namely, $\hat{Y}$, which adversely affects any future measurements of the observable. This noise is called the measurement backaction noise and was initially evaded by making an effective joint quadrature measurement of the system [38,61,62]. This technique enables the possibility of conducting the quantum nondemolition measurement [63], where measurement does not affect the observed system. The use of backaction evasion was used to overcome the SQL in optomechanics [64], with the technique later being expanded for two-mode measurements [65,66]. Further theoretical development has focused on BAE schemes beyond the rotating-wave approximation (RWA) to include the effect of counterrotating terms [48–50].

For backaction evasion, a bichromatic laser beam with two frequencies $\omega_{\mp} = \omega_a \pm \delta$ is injected into the cavity [47] that contains the BEC in a ring trap, where $\delta = \omega_m = (\omega_c + \omega_d)/2$ is the average frequency of the two atomic sideband modes. The optical fields oscillate with amplitudes $\varepsilon_{\pm}$. The Hamiltonian is given by

$$H/\hbar = \omega_a a^\dagger a + \omega_c c^\dagger c + \omega_d d^\dagger d + G a^\dagger a (X_c + X_d) + (a\varepsilon_+^* e^{i(\omega_a - \omega_m)t} + a\varepsilon_-^* e^{i(\omega_a + \omega_m)t} + \text{H.c.}), \quad (17)$$

where we have ignored the terms due to collisions as they only cause a relative shift in the frequencies and have no significant impact on sensitivity. Moving to the driving frame, $a = e^{-i\omega_a t}[\bar{a}(e^{-i\delta t} + e^{i\delta t}) + \delta a]$, where $\bar{a}$ and δa are the steady state and fluctuations of the cavity field and δ is the detuning. The linearization of the operator a around a monostable steady state is shown in Appendix D. An effective Hamiltonian $H_{\rm eff}$ is then obtained, which is given by

$$H_{\rm eff}/\hbar = (\omega_m + \Omega)c^\dagger c + (\omega_m - \Omega)d^\dagger d + 2G\bar{a}\cos\delta t (X_c + X_d)(\delta a^\dagger + \delta a). \quad (18)$$

Here $\Omega = (\omega_c - \omega_d)/2$ and $\delta = \omega_m$ at resonance. In the frame rotating with ω_m, the atomic sideband modes oscillate with frequencies $\pm\Omega$, and the spectral response will show peaks at these frequencies. The winding number L_p of the BEC in the annular trap can be measured using the relation

$$\Omega = \frac{\omega_c - \omega_d}{2} = \frac{\hbar(L_p + 2l)^2}{4I} - \frac{\hbar(L_p - 2l)^2}{4I} = \frac{2L_p l\hbar}{I}, \quad (19)$$

where I and l are assumed to be known.

The effect of BAE becomes clear under the RWA, where the effective Hamiltonian reduces to a time-independent Hamiltonian, as $2G\bar{a}\cos(\delta t) = 2G\bar{a}$, and under the transformation $U = e^{i\omega_m(c^\dagger c + d^\dagger d)t}$ can be written as ($\hbar = 1$)

$$H'_{\rm eff} = \Omega(c^\dagger c - d^\dagger d) + 2G\bar{a}\cos\delta t (X_c + X_d)(\delta a^\dagger + \delta a).$$

Now by transforming to a set of symmetric and antisymmetric quadratures $X_\pm = (X_c \pm X_d)/\sqrt{2}$ and $P_\pm = (P_c \pm P_d)/\sqrt{2}$, we get

$$H'_{\rm eff} = \Omega(X_+X_- + P_+P_-) + \bar{G}X_+\delta Q, \quad (20)$$

where $\bar{G} = 2\sqrt{2}G\bar{a}$, $\delta Q = (\delta a + \delta a^\dagger)/\sqrt{2}$, and $\delta P = i(\delta a^\dagger - \delta a)/\sqrt{2}$. The equation of motion of the system is then given by

$$\delta\dot{Q} = -\frac{\kappa}{2}\delta Q + \sqrt{\kappa}Q_{\rm in}, \quad \dot{X}_\pm = \Omega P_\mp, \quad (21)$$

$$\delta\dot{P} = -\frac{\kappa}{2}\delta P + \sqrt{\kappa}P_{\rm in} + \sqrt{2}G\bar{a}X_+\delta Q. \quad (22)$$

As shown in Fig. 5, measurement of the variable P is dependent on X_+, but the measurement backaction on the conjugate variable P_+ is decoupled from the dynamics of X_+, thus allowing a perfect backaction evasion measurement.

Beyond the RWA, the decoupling of quadratures is not necessarily perfect so as to allow quantum nondemolition measurements, but can still significantly alleviate the effects of backaction noise. The key step here is to solve the time-dependent effective Hamiltonian derived in Eq. (18). Using the input noise operators and losses from Sec. III, the quantum Langevin equations for the BAE scheme can be written as [47]

$$\delta\dot{a} = -\frac{\kappa}{2}\delta a + \sqrt{\kappa}a_{\rm in} + 2iG\bar{a}\cos(\delta t)(X_c + X_d)(\delta a + \delta a^\dagger), \quad (23)$$

$$\ddot{X}_{c\,(d)} = (\omega_m \pm \Omega)^2 X_{c\,(d)} + 2G\bar{a}\cos(\delta t)(\omega_m \pm \Omega) \times(\delta a + \delta a^\dagger) - \gamma\dot{X}_{c\,(d)} + (\omega_m \pm \Omega)\epsilon_{c\,(d),\rm in}. \quad (24)$$

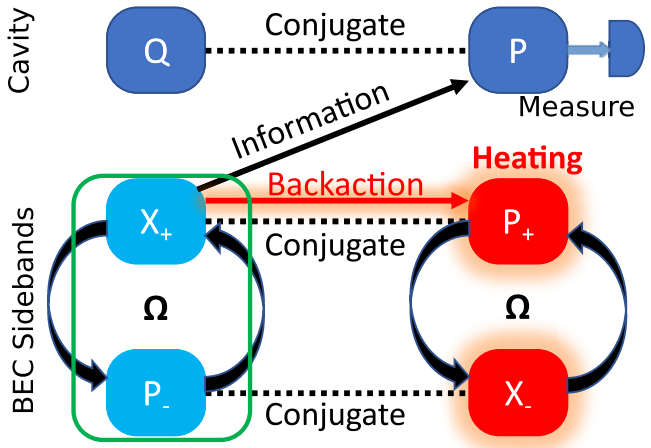

FIG. 5. Schematic showing the BAE scheme. Measurement of the cavity observable P requires information from the X_+ variable of the BEC. The backaction of the measurement is transferred to the conjugate variable P_+, which is dynamically decoupled from the subspace of X_+ and P_-. Therefore, P can be continuously measured as the evolution of X_+ is unaffected by backaction.

In terms of the optical quadrature variables $\{Q_{\rm in}, P_{\rm in}\}$, defined in Eq. (6), Eq. (23) can be written as

$$\delta\dot{P} = -\frac{\kappa}{2}\delta P + \sqrt{\kappa}P_{\rm in} + 4G\bar{a}\cos(\delta t)\delta Q(X_c + X_d),$$
$$\delta\dot{Q} = -\frac{\kappa}{2}\delta Q + \sqrt{\kappa}Q_{\rm in}. \tag{25}$$

To obtain the solution for the time-dependent equations of motion beyond the RWA, we consider an approach [48,49] based on the Floquet expansion of the dynamical variables. The formalism is valid even in the bad cavity regime, i.e., for $\omega_{c\,(d)} \ll \kappa$, as the couplings are also small $G \ll \kappa$. Applying the Floquet expansion to each dynamical variable $Z(t)$ as $Z(t) = \sum_{-\infty}^{\infty} Z^{(n)}(t)e^{in\delta t}$, the variables can be transformed to the frequency domain, by applying the Fourier transform of the above equations. Equating the terms with $e^{in\delta t}$ and considering the noise terms to be stationary ($n = 0$), the expressions for the quadratures fluctuations are obtained,

$$\chi_c^{-1}(\omega - n\delta)X_c^{(n)}(\omega) = \{G\bar{a}[\delta Q^{(n-1)} + \delta Q^{(n+1)}(\omega)] + \epsilon_{c,\rm in}(\omega)\}(\omega_m + \Omega), \tag{26}$$

$$\chi_a^{-1}(\omega - n\delta)\delta Q^{(n)}(\omega) = -\delta_{n,0}\sqrt{\kappa}Q_{\rm in}(\omega), \tag{27}$$

$$\chi_a^{-1}(\omega - n\delta)\delta P^{(n)}(\omega) = -\delta_{n,0}\sqrt{\kappa}P_{\rm in}(\omega) + G\bar{a}\sqrt{2}(X_c^{(n-1)} + X_c^{(n+1)} + X_d^{(n-1)} + X_d^{(n+1)}), \tag{28}$$

$$\chi_a^{-1}(\omega - n\delta)a^{(n)}(\omega) = -\delta_{n,0}\sqrt{\kappa}\,a_{\rm in}(\omega) - iG\bar{a}(X_c^{(n-1)} + X_c^{(n+1)} + X_d^{(n-1)} + X_d^{(n+1)}), \tag{29}$$

where $\chi^{-1}_{a,c(d)}$ are the susceptibilities defined in Sec. III. Now the expressions obtained by solving these are

$$\delta P^{(0)}(\omega) = \chi_a^2(\omega)\sqrt{2}G^2\bar{a}^2\kappa Q_{\rm in}^{(0)}(\omega)[\chi_c(\omega - \delta) + \chi_c(\omega + \delta) + \chi_d(\omega - \delta) + \chi_d(\omega + \delta)], \tag{30}$$

$$\delta P^{(1)}(\omega) = \chi_a(\omega - \delta)G\bar{a}\sqrt{2\kappa}[\chi_c(\omega)(\omega_m + \Omega)\epsilon_{c,\rm in}^{(0)}(\omega) + \chi_d(\omega)(\omega_m - \Omega)\epsilon_{d,\rm in}^{(0)}(\omega)], \tag{31}$$

$$\delta P^{(-1)}(\omega) = \chi_a(\omega + \delta)G\bar{a}\sqrt{2\kappa}[\chi_c(\omega)(\omega_m + \Omega)\epsilon_{c,\rm in}^{(0)} + \chi_d(\omega)(\omega_m - \Omega)\epsilon_{d,\rm in}^{(0)}(\omega)], \tag{32}$$

$$\delta P^{(2)}(\omega) = \sqrt{2}\chi_a(\omega - 2\delta)G^2\bar{a}^2\chi_a(\omega)[\chi_c(\omega - \delta) + \chi_d(\omega - \delta)]\sqrt{\kappa}Q_{\rm in}^{(0)}(\omega), \tag{33}$$

$$\delta P^{(-2)}(\omega) = \sqrt{2}\chi_a(\omega + 2\delta)G^2\bar{a}^2\chi_a(\omega)[\chi_c(\omega + \delta) + \chi_d(\omega + \delta)]\sqrt{\kappa}Q_{\rm in}^{(0)}(\omega), \tag{34}$$

$$\delta P^{(3)}(\omega) = 0, \quad \delta P^{(-3)}(\omega) = 0,$$
$$\delta Q^{(n)}(\omega) = \delta_{n,0}\sqrt{\kappa}\chi_a(\omega)Q_{\rm in}^{(0)}(\omega). \tag{35}$$

Importantly, the fact that the input quantum and thermal noise is stationary, i.e., only the zeroth Floquet mode ($n = 0$) is nonzero, ensures that the series truncates at $|n| = 3$ for all noise quadratures. From Eq. (27) note that $\delta Q^{(n)}$ is nonzero only for $n = 0$, which implies that modes in quadrature $\delta X_c^{(n)}$ in Eq. (26) are $n = 0, \pm 1$. Hence, the operators $\delta P^{(n)}$ and $a^{(n)}$ in Eqs. (28) and (29) have Floquet modes only for $n = 0, \pm 1, \pm 2$. As such, for stationary noise, the optical susceptibilities for frequency $\omega - n\delta$ can at most add up to the second harmonics (0, $\omega \pm \delta$, and $\omega \pm 2\delta$), giving rise to a contribution from only a finite set of sideband modes. This reduces the complexity in solving the problem and in fact allows for exact solutions to be obtained for the noise quadrature fluctuations. The nonzero Floquet components are then used to calculate the zeroth-order spectral density, which represents the average optical spectrum. The spectral response function will allow us to directly estimate the rotational properties of the BEC.

Now to obtain the output spectrum, the input-output formalism is again used. Let $\{A(\omega), B(\omega), C(\omega), D(\omega)\}$ be the frequency-dependent coefficients of the noise quadrature operators $Q_{\rm in}$, $P_{\rm in}$, $\epsilon_{c,\rm in}$, and $\epsilon_{d,\rm in}$, respectively, in Eqs. (30)–(35). The expressions for these coefficients are shown in Appendix E. The homodyne detection angle is set at $\phi = \pi/2$, as the noise spectrum is analyzed using the noise quadrature $P_{\rm out}(\omega)$, which is given by

$$P_{\rm out}^{(n)}(\omega) = A^{(n)}(\omega)Q_{\rm in}(\omega) + B^{(n)}(\omega)Q_{\rm in}(\omega) + C^{(n)}(\omega)\epsilon_{c,\rm in}(\omega) + D^{(n)}(\omega)\epsilon_{d,\rm in}. \tag{36}$$

The Fourier components of the spectrum [48] are given by the expression

$$S_{A^\dagger A}^{(m)}(\omega) = \sum_n \int \frac{d\omega'}{2\pi}\langle A^{(n)\dagger}(\omega + n\delta)A^{(m-n)}(\omega')\rangle, \tag{37}$$

where the time-averaged noise spectrum is captured by the zeroth Fourier component ($n = 0$) of the above spectrum,

given by

$$S^{(0)}_{A^\dagger A}(\omega) = \sum_n \int \frac{d\omega'}{2\pi} \langle A^{(n)\dagger}(\omega + n\delta) A^{(-n)}(\omega') \rangle. \tag{38}$$

Using Eqs. (30)–(35) and the coefficients in Eq. (36), the expression for the spectral density is

$$\begin{aligned} S^{\text{out}}_{P,P}(\omega) = \frac{1}{2}[&A^{-2}(\omega + 2\delta) A^{+2}(-\omega - 2\delta) \chi_{QQ}(\omega + 2\delta) \\ &+ C^{-1}(\omega + \delta) C_1(\omega - \delta) \chi_{cc}(\omega + \delta) \\ &+ D^{-1}(\omega + \delta) D_1(-\omega - \delta) \chi_{dd}(\omega + \delta) \\ &+ A^{2}(\omega - 2\delta) A^{-2}(-\omega + 2\delta) \chi_{QQ}(\omega - 2\delta) \\ &+ C^{1}(\omega - \delta) C_{-1}(\omega + \delta) \chi_{cc}(\omega - \delta) \\ &+ D^{1}(\omega - \delta) D^{-1}(-\omega + \delta) \chi_{dd}(\omega - \delta)] \\ &+ \frac{1}{2}[A^0(\omega) A^0(-\omega) \chi_{QQ}(\omega) + B^0(\omega) B^0(-\omega) \chi_{PP} \\ &+ A^0(\omega) B^0(-\omega) \chi_{QP} + B^0(\omega) A^0(-\omega) \chi_{PQ}], \end{aligned} \tag{39}$$

where $\chi_{i,j}(\omega)$ are the input noise correlations between i and j modes such that $i, j \in \{c_{\text{in}}(\omega), d_{\text{in}}(\omega), Q_{\text{in}}(\omega), P_{\text{in}}(\omega)\}$. Figure 6(a) shows the output spectral function $S^{\text{out}}_{P,P}(\omega)$ for different values of the input power $\mathcal{P}_{\text{in}} = \mathcal{P}_\pm$, with the peak occurring at $\omega = \Omega$. The peak is directly related to the winding number L_p of the BEC and is sharper for higher input power imbalance. The measurement sensitivity is given by $\zeta(\omega)$ defined in Eq. (13), where the optomechanical measurement time is given by $t^{-1}_{\text{meas}}(\omega) = |\sqrt{2\kappa} G\bar{a}/(-i\omega + \kappa/2)|^2$. This is defined as the absolute value of the rate at which the output quadrature mode $P^{(0)}_{\text{out}}$ changes with respect to the mechanical fluctuations $\delta X^{(\pm 1)}_{c\,(d)}$. In Fig. 6(b) the sensitivity ζ is varied with frequency ω for different input powers $\mathcal{P}_\pm$. Similar to the squeezed input case, the maximum sensitivity occurs at two points in the close vicinity of the spectral peak Ω. The optimal frequency ω_{opt} can then be used to precisely sense the angular momentum of the rotating BEC inside the cavity.

The sensitivity of the backaction evasion measurements can be enhanced and the output noise lowered by adding squeezing to the bichromatic drive [51]. As in Sec. III, in this case the squeezing is introduced through the input noise correlations, with amplitude r and angle θ. The enhancement of sensitivity with squeezed light in the BAE method is shown in Fig. 7 for different parameter regimes. In all cases, the enhancement factor is the ratio of the optimal sensitivity with and without squeezed light in the backaction evasion approach, varied along with some other parameter such as power or OAM of the input light.

For instance, in Fig. 7(a) the enhancement factor is $\zeta_{\text{opt}}(0,0)/\zeta_{\text{opt}}(r,\theta)$, which shows the variation of enhancement with r and θ. It is observed that $\theta = \pi$ always generates the maximum sensitivity and is thus fixed for all the other plots. In Fig. 7(b) the variation of the enhancement factor with the input power $\mathcal{P}_{\text{in}}$ and squeezing amplitude r is shown. At low squeezing, the sensitivity decreases with higher power and the enhancement factor can increase by nearly two orders of magnitude. Importantly, at high $\mathcal{P}_{\text{in}}$, where the radiation pressure noise is dominant, the effect of squeezing becomes marginal. The variation of the enhancement factor with the OAM number l of the input light is shown in Fig. 7(c), where it is evident that enhancement is higher for larger values of l and r. Finally, the enhancement in sensitivity is shown to only marginally change for different values of the angular momentum of the condensate $L_p\hbar$, as shown in Fig. 7(d).

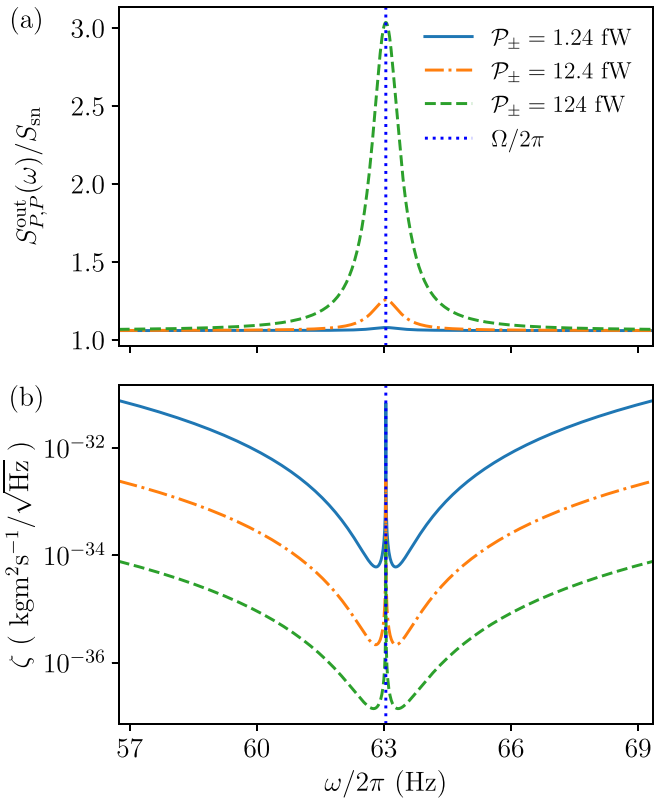

FIG. 6. Output noise spectrum and measurement sensitivity for the BAE scheme. The plots are for different values of $\mathcal{P}_{\text{in}} = \mathcal{P}_\pm$, where $\mathcal{P}_+ = \mathcal{P}_-$ is the same input power for the two driving fields in the BAE scheme. (a) Output optical spectrum $S^{\text{out}}_{P,P}(\omega)$ for different driving frequencies ω, with a peak at frequency $\Omega/2\pi = 63$ Hz. The plots have been scaled with the shot noise at different powers for ease of viewing, with $S_{\text{sn}} = 10, 1, 0.1$ (in units of $\{\text{\rm Hz}\}^{-1}$) for increasing power. (b) Variation in sensitivity with ω, with minimal sensitivity occurring at two optimal points ω_{opt}, in the vicinity of the spectral peak. The detection angle is set at $\phi = \pi/2$. The other parameters are the same as in Fig. 2.

The variation of the output noise spectral density $S^{\text{out}}_{P,P}(\omega)$ at the optimal frequency $\omega = \omega_{\text{opt}}$ with the input power $\mathcal{P}_{\text{in}}$ is shown in Fig. 8. While the spectral density could only be lowered below the minimum noise at temperature $T_{c,d}$ using squeezed light (see Fig. 4), using the backaction evasion method, the noise can be lowered well beyond the SQL. This is achieved by significantly lowering the radiation pressure noise through the backaction evasion method, which is typically more prominent at higher input powers. In contrast, at lower input powers, where the shot noise is more dominant, the noise spectrum is not significantly lowered. However, by introducing squeezing in the input bichromatic drive of the BAE scheme, the shot-noise barrier can be broken and

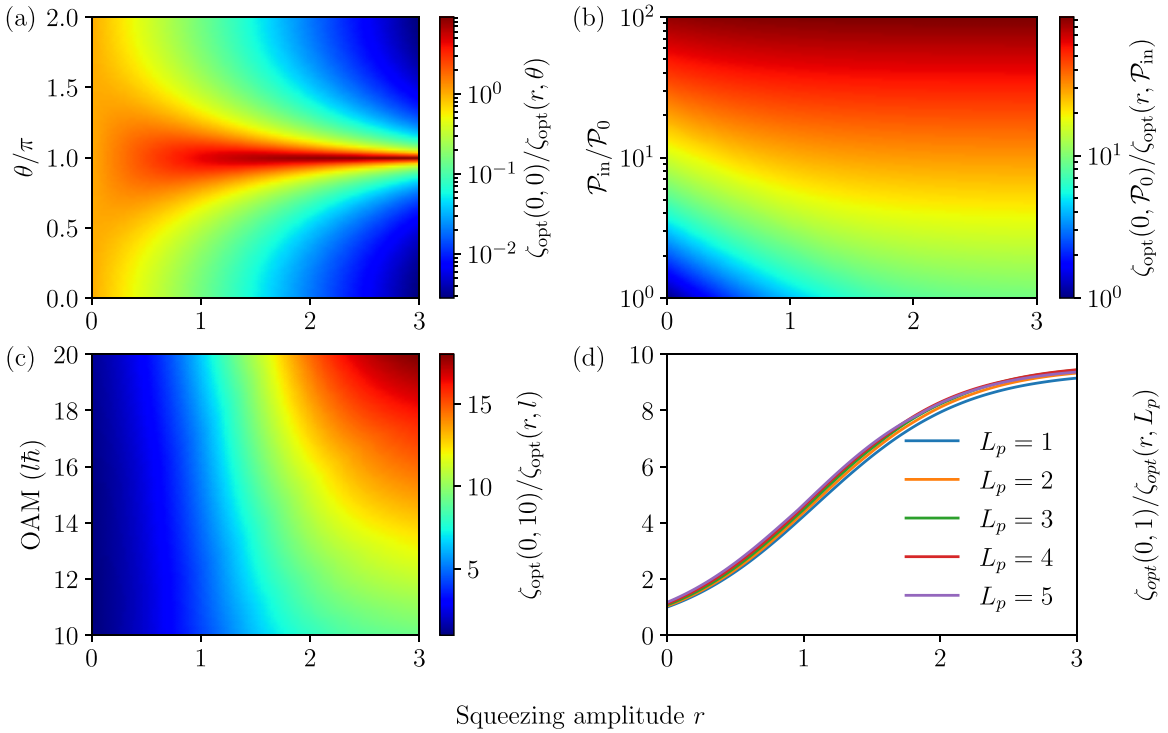

FIG. 7. Enhancement of optimal sensitivity in the BAE scheme using squeezed input light. The plot shows the enhancement as a function of squeezing amplitude r and (a) squeezing angle θ, (b) relative input power $\mathcal{P}_{\rm in}/\mathcal{P}_0$, (c) OAM of the input light $l\hbar$, and (d) the winding number of the atomic condensate L_p. The input power $\mathcal{P}_{\rm in} = \mathcal{P}_0 = 12.4$ fW and $l = 10$, unless varied. All the other parameters are the same as in Fig. 2.

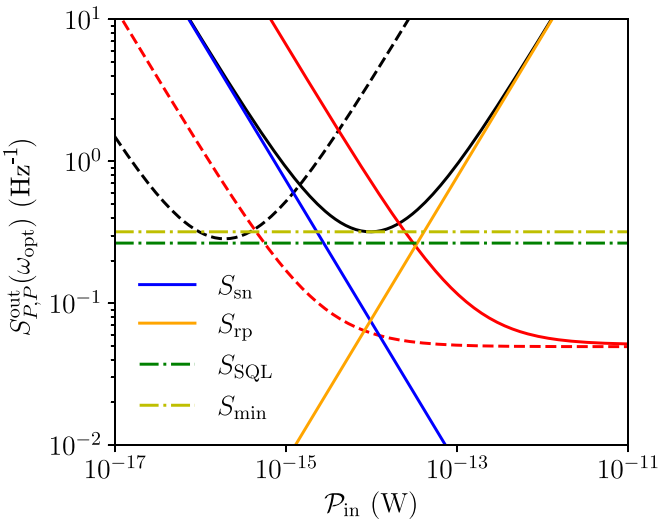

FIG. 8. Output spectrum with input power for the BAE scheme. The output spectrum (black solid curve), due to the contributions from shot noise (blue solid line), radiation pressure (orange solid line), and thermal and quantum fluctuations, reaches the minimum value $S_{\rm min}$ (green dash-dotted line) at input power $\mathcal{P}^{\rm opt}_{\rm in}$. The spectrum due to the backaction evasion scheme (red solid line) is significantly lower than the standard quantum limit (light green dash-dotted line) at higher input powers. For squeezed input in bichromatic BAE driving, with $r = 2$ and $\theta = \pi$, the spectrum can break the SQL even at lower $\mathcal{P}_{\rm in}$ (red dashed curve). All the other parameters are the same as in Fig. 2.

noise beyond the SQL can be achieved even at lower input powers.

An important result in the detection of rotational properties of the BEC is the trade-off involved in achieving enhanced sensitivity using squeezed light and, on the other hand, lowering the noise spectral density far beyond the SQL using nondemolition measurements such as the backaction evasion method. This is evident from the sensitivity enhancement for the two different protocols, as observed in Fig. 9 for a wide range of input powers $\mathcal{P}_{\rm in}$. The enhancement is in comparison to the initial case where a monochromatic, unsqueezed OAM beam is injected into the cavity and interacts with the condensate. At lower input powers, where the shot noise is dominant, the effect of using squeezing in the OAM of light on the sensitivity of measurements is quite strong and an enhancement of 18 dB can be observed. However, for input powers above $\mathcal{P}_{\rm in} = \mathcal{P}_0$, there is no enhancement in sensitivity. The use of backaction evasion to lower the noise beyond the SQL seems to have the opposite effect on measurement sensitivity, especially at lower powers. The bichromatic drive in the BAE method broadens the noise spectral density and makes it significantly less sensitive. However, if squeezing is added to the BAE scheme, sensitivity enhancement of 2–3 dB is observed at low powers. Importantly, at $\mathcal{P}_{\rm in} = \mathcal{P}_0$ the sensitivity is as good as the non-BAE approaches, and hence the noise can be lowered without negatively affecting the sensitivity of the measurements. At powers above $\mathcal{P}_{\rm in} \sim 1$ pW, none of the approaches provide any enhancement over the initial case.

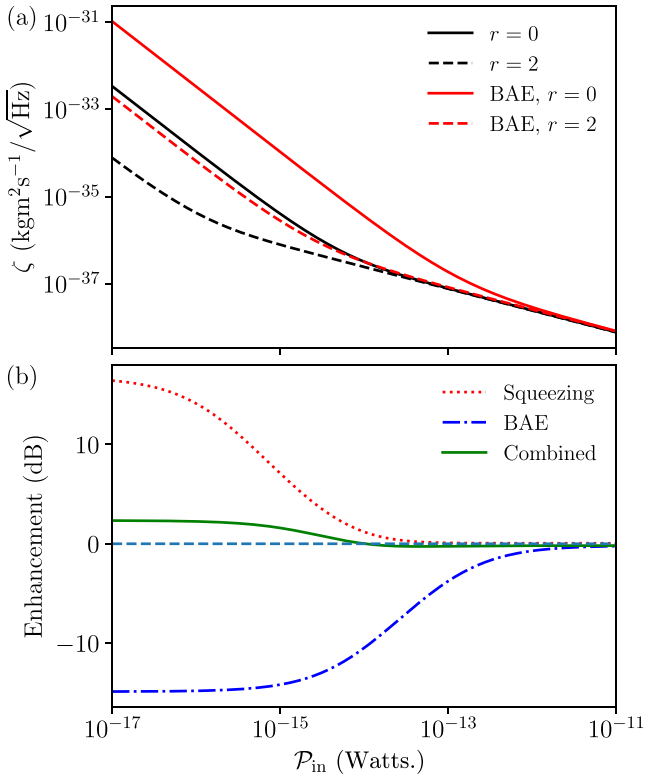

FIG. 9. Sensitivity and its enhancement for different values of input power $\mathcal{P}_{\text{in}}$. (a) Sensitivity with (red solid line) and without (black solid line) the BAE approach. The effect of squeezing in each case is shown by the dashed line. (b) Enhancement in sensitivity due to squeezed input alone (red dotted line), the BAE approach (blue dash-dotted line), and BAE with additional squeezing (green solid solid), in comparison to driving the cavity with only OAM light. For all input $l = 10$ and for squeezed noise $r = 2$ and $\theta = \pi$. All the other parameters are the same as in Fig. 2.

V. CONCLUSION

In this work we have analyzed the measurement of the rotation of an atomic BEC in a ring trap, such as its winding number, using cavity modes carrying orbital angular momentum, in a minimally destructive manner. The interaction between the sidemodes of the BEC and the light carrying OAM reduces to a set of optomechanical equations of motion, which typically allows for sensing of the angular momentum close to the standard quantum limit.

By exploiting the theoretical framework of optomechanics, we have shown that the quantum sensing of such rotational properties can be significantly enhanced. The introduction of squeezed light as input, and for optimal homodyne detection angles, the sensitivity of detecting the spectral peaks of the output light and therefore the angular momentum can be enhanced by a factor of 2–100 (approximately equal to 4–20 dB) as compared to unsqueezed input. Notably, the higher enhancement occurs only at low input powers, where the shot noise is dominant. Moreover, the optical quadrature noise, at optimal frequencies ω, is observed to go below the shot noise and break the minimum noise level at temperature $T_{c,d}$, which was hitherto the best that could have been achieved using OAM light as input, without any squeezing.

The noise spectral density can be reduced below the SQL by using backaction evasion methods to counter the radiation pressure or measurement backaction noise at high input powers. This was achieved by using a bichromatic drive, which yields a spectral peak at a frequency directly related to the winding number of the BEC. Using an approach based on Floquet theory to solve the time-dependent dynamics, the output noise spectral density was calculated in the bad cavity regime and beyond the rotating-wave approximation. It was observed that the backaction evasion allowed the output noise spectral density to be lowered beyond the standard quantum limit, albeit at the cost of measurement sensitivity. However, using squeezed light in the bichromatic drive of the backaction evasion method, the overall measurement sensitivity was improved, and at relevant input powers, the sensitivity was restored to non-BAE levels with SQL being broken even at lower input powers. Ultimately, the use of squeezing in the BAE scheme allowed for very precise measurements of rotational properties of the BEC, with noise well below the standard quantum limit.

The framework introduced in the study is quite extensive and can be applied to investigate other properties and phenomena related to the study of atomic superfluids and its interaction with nonclassical light. We expect our results to be relevant to ongoing studies of superfluid hydrodynamics, and the sensing and manipulation of rotating matter waves. Of further interest is the role of ponderomotive squeezing introduced in the scattered atomic sidemodes and the resulting entanglement in the system. Moreover, full quantum solutions in systems with low excitations can allow for applications that are directly related to quantum technology such as generation of entangled light, coherent transfer of information between the collective states of light and matter, and implementation of lower-power quantum devices.

ACKNOWLEDGMENTS

R.G. acknowledges financial support from CSIR-HRDG, India in the form of SRF. P.K. acknowledges financial support from the Max Planck Society. M.B. would like to thank the U.S. Air Force Office of Scientific Research for support through Grant No. FA9550-23-1-0259. R.K. acknowledges support from JSPS KAKENHI Grant No. JP21K03421. H.S.D. acknowledges support from SERB-DST, India under Core-Research Grant No. CRG/2021/008918 and from IRCC, IIT Bombay through Grant No. RD/0521-IRCCSH0-001.

APPENDIX A: SCATTERING OF THE BEC WITH AN OPTICAL LATTICE FORMED BY OAM BEAMS

As stated in Sec. II, the cavity is injected with a single-mode symmetric superposition of OAM light given by $|+\rangle = |+l\hbar\rangle + |-l\hbar\rangle$ (with annihilation operator a). The light-matter interaction varies azimuthally as approximately $\cos^2(l\varphi)a^\dagger a$. This changes the spatial mode of BEC from L_p

as follows:

$$\begin{aligned}\cos^2(l\varphi)|L_p\rangle &= \left(\frac{1+\cos(2l\varphi)}{2}\right)|L_p\rangle,\\ &= \frac{1}{2}|L_p\rangle + \frac{1}{4}(e^{i2l\varphi}+e^{-i2l\varphi})|L_p\rangle,\\ &= \frac{1}{2}|L_p\rangle + \frac{1}{4}(|L_p+2l\rangle + |L_p-2l\rangle). \quad \text{(A1)}\end{aligned}$$

In the last line, we have used the fact that the exponential of the angular displacement operator φ is the generator of angular momentum translations. Now the BEC order parameter in the position representation is given by

$$\begin{aligned}\Phi(\varphi) &\sim \langle\varphi|\cos^2(l\varphi)|L_p\rangle \sim \frac{1}{2}\langle\varphi|L_p\rangle\\ &+ \frac{1}{4}(\langle\varphi|L_p+2l\rangle + \langle\varphi|L_p-2l\rangle)\\ &\sim \frac{e^{iL_p\varphi}}{2} + \frac{e^{i(L_p+2l)\varphi}+e^{i(L_p-2l)\varphi}}{4}\\ &\sim \frac{e^{iL_p\varphi}}{2}[1+\cos(2l\varphi)]. \quad \text{(A2)}\end{aligned}$$

The density is given by $n(\varphi)\sim|\Phi(\varphi)|^2\sim[1+\cos(2l\varphi)]^2$, which shows that only the $\cos(2l\varphi)$ and $\cos(4l\varphi)$ density modes are populated by scattering from the $|+\rangle$ mode.

Importantly, sine density modes, which correspond to light-matter interaction arising from antisymmetric superposition of OAM light $|-\rangle = |+l\hbar\rangle - |-l\hbar\rangle$, are not present if only first-order Bragg scattering processes are considered. In fact, since higher-order scattering terms involve repetitive action of $\cos^2(l\varphi)$ on the scattered states, these processes also do not introduce sine mode density excitations. However, interference between the persistent currents can introduce sine modes. Nonetheless, these condensate excitations cannot transfer photons out from the $|+\rangle$ mode to any other optical mode, since Bragg scattering involves stimulated emission, which can repopulate only the $|+\rangle$ mode [67]. Photons can be scattered into modes other than $|+\rangle$ only via spontaneous emission. However, for the large light-atom detunings considered in this work, spontaneous emission is negligible [14,26]. Thus, we only consider the $|+\rangle$ optical mode in our model.

APPENDIX B: COEFFICIENTS OF OUTPUT QUADRATURES

To obtain the output optical quadrature $\delta P(\omega)$ and $\delta Q(\omega)$, the equation $\mathcal{F}\delta u = Du_{\rm in}$ needs to be solved, which requires inverting the matrix $\mathcal{F}$ in Eq. (9). Solving the equation and following the input-output formalism, the coefficients for the quadratures are obtained,

$$\begin{aligned}P_{\rm out}(\omega) &= A_P(\omega)Q_{\rm in}(\omega) + B_P(\omega)Q_{\rm in}(\omega)\\ &+ C_P(\omega)\epsilon_{c,\rm in}(\omega) + D_P(\omega)\epsilon_{d,\rm in}, \quad \text{(B1)}\end{aligned}$$

$$\begin{aligned}Q_{\rm out}(\omega) &= A_Q(\omega)Q_{\rm in}(\omega) + B_Q(\omega)P_{\rm in}(\omega)\\ &+ C_Q(\omega)\epsilon_{c,\rm in}(\omega) + D_Q(\omega)\epsilon_{d,\rm in}, \quad \text{(B2)}\end{aligned}$$

where $\{A_{P\,(Q)}, B_{P\,(Q)}, C_{P\,(Q)}, D_{P\,(Q)}\}$ are the output optical quadrature coefficients for respective components of $\{Q_{\rm in}, P_{\rm in}, \epsilon_c, \epsilon_d\}$. The coefficients satisfy $A_P/A'_P = C_P/C'_P = D_P/D'_P$, $B_Q/B'_Q = C_Q/C'_Q = D_Q/D'_Q = \sqrt{\kappa}$, and $A_Q/A'_Q = B_P/B'_P = \sqrt{\kappa}-1$, where

$$A'_Q(\omega) = \chi_a\sqrt{\gamma_o}(\mathcal{A}^2\chi_c\chi_d+1)/\mathcal{D}(\omega), \quad \text{(B3)}$$

$$B'_Q(\omega) = -\Delta'\chi_a^2\sqrt{\gamma_o}(\mathcal{A}^2\chi_c\chi_d+1)/\mathcal{D}(\omega), \quad \text{(B4)}$$

$$C'_Q(\omega) = \sqrt{2}\Delta' G a_s\chi_a^2\chi_c\omega_c(\mathcal{A}\chi_d+1)/\mathcal{D}(\omega), \quad \text{(B5)}$$

$$D'_Q(\omega) = \sqrt{2}\Delta' G a_s\chi_a^2\chi_d\omega_d(1-\mathcal{A}\chi_c)/\mathcal{D}(\omega), \quad \text{(B6)}$$

$$\begin{aligned}A'_P(\omega) = \big(\sqrt{\gamma_o}\chi_a^2\big\{\chi_c\big[2G^2a_s^2\tilde{\omega}_c(\mathcal{A}\chi_d+1)+\mathcal{A}^2\Delta'\chi_d\big]\\ -2G^2a_s^2\chi_d\tilde{\omega}_d(\mathcal{A}\chi_c-1)+\Delta'\big\}\big)/\mathcal{D}(\omega), \quad \text{(B7)}\end{aligned}$$

$$B'_P(\omega) = \chi_a\sqrt{\gamma_o}(\mathcal{A}^2\chi_c\chi_d+1)/\mathcal{D}(\omega), \quad \text{(B8)}$$

$$C'_P(\omega) = -\sqrt{2}G a_s\chi_a\chi_c\omega_c(\mathcal{A}\chi_d+1)/\mathcal{D}(\omega), \quad \text{(B9)}$$

$$D'_P(\omega) = \sqrt{2}G a_s\chi_a\chi_d\omega_d(\mathcal{A}\chi_c-1)/\mathcal{D}(\omega), \quad \text{(B10)}$$

$$\begin{aligned}\mathcal{D}(\omega) = \Delta'\chi_a^2\big\{\chi_c\big[2G^2a_s^2\tilde{\omega}_c(\mathcal{A}\chi_d+1)+\mathcal{A}^2\Delta'\chi_d\big]\\ -2G^2a_s^2\chi_d\tilde{\omega}_d(\mathcal{A}\chi_c-1)+\Delta'\big\}+\mathcal{A}^2\chi_c\chi_d+1.\end{aligned} \quad \text{(B11)}$$

APPENDIX C: OPTIMAL HOMODYNE DETECTION ANGLE FOR THE NOISE SPECTRUM AND SENSITIVITY

For the homodyne detection, one can define generalized quadratures with respect to an angle ϕ. The output spectral density for the generalized quadrature is given by Eq. (11) and the different components are given by $S^{\rm out}_{Q^\phi,Q^\phi} = S^\phi(\omega) = \cos^2\phi S_{QQ} + \sin^2\phi S_{PP} + \cos\phi\sin\phi(S_{QP}+S_{PQ})$. To maximize this spectral density, $\partial S^\phi/\partial\phi = 0$, with $\partial^2 S^\phi/\partial\phi^2 < 0$, which gives

$$\begin{aligned}\frac{\partial S^\phi}{\partial\phi} &= \sin 2\phi(S_{PP}-S_{QQ}) + \cos 2\phi(S_{QP}+S_{PQ})\\ &= 0 \Rightarrow \phi = \frac{1}{2}\tan^{-1}\left(\frac{S_{QP}+S_{PQ}}{S_{QQ}-S_{PP}}\right), \quad \text{(C1)}\\ \frac{\partial^2 S^\phi}{\partial\phi^2} &= 2\cos 2\phi[S_{PP}-S_{QQ}-\tan 2\phi(S_{QP}+S_{PQ})]\\ &< 0 \Rightarrow \frac{S_{PP}-S_{QQ}}{S_{QP}+S_{PQ}} < \tan 2\phi. \quad \text{(C2)}\end{aligned}$$

Using the relations (C1) and (C2),

$$\begin{aligned}&\frac{S_{PP}-S_{QQ}}{S_{QP}+S_{PQ}} < \frac{S_{QP}+S_{PQ}}{S_{QQ}-S_{PP}}, \quad \text{(C3)}\\ &\Rightarrow -(S_{PP}-S_{QQ})^2 < (S_{QP}+S_{PQ})^2,\\ &\Rightarrow (S_{QP}+S_{PQ})^2 + (S_{PP}-S_{QQ})^2 > 0, \quad \text{(C4)}\end{aligned}$$

$$S^\phi(\omega) = \frac{1}{2}(S_{QQ}+S_{PP}) + \frac{1}{2}\sqrt{(S_{QQ}-S_{PP})^2+(S_{QP}+S_{PQ})^2}. \quad \text{(C5)}$$

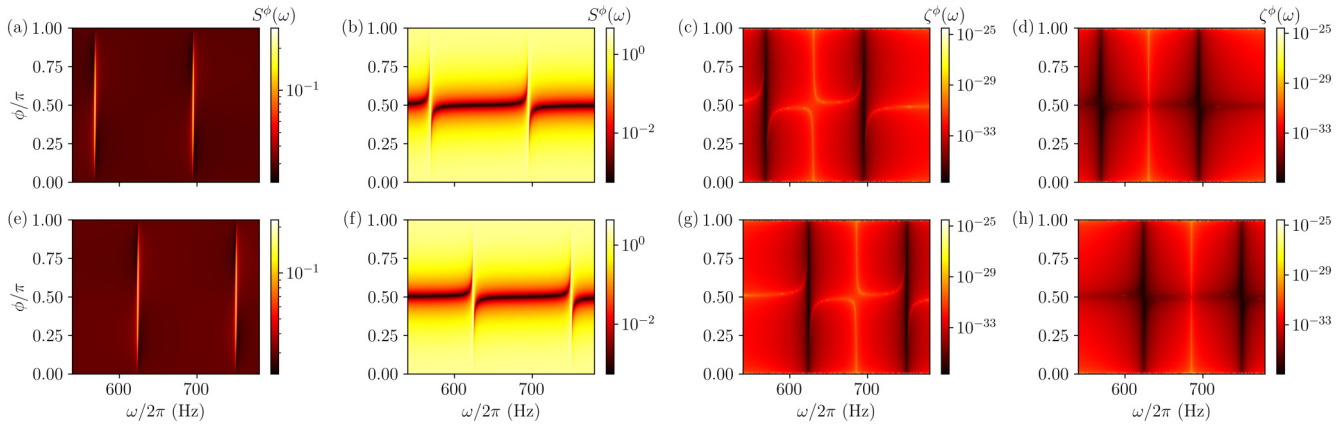

FIG. 10. Variation of the output optical spectrum and sensitivity with detection angle ϕ: (a) and (e) output spectrum and (c) and (g) sensitivity for unsqueezed input light and (b) and (f) output spectrum and (d) and (h) sensitivity for squeezed input with amplitude $r = 2$ and angle $\theta = \pi$, for the cases (a)–(d) with and (e)–(h) without interatomic interaction or collisions.

For unsqueezed input, $S_{QP} = -S_{PQ}$ and $S_{PP} > S_{QQ}$, which gives the detection angle $\phi_0 = \pi/2$ for the optimal noise spectrum. Therefore, $Q^{\phi}_{\rm out} = P_{\rm out}$ and $S^{\phi} = S^{\rm out}_{P,P}$. However, the above conditions for optimal ϕ may vary if squeezed input is used.

Figure 10 shows the numerical results for the spectral density $S^{\phi}(\omega)$ and the sensitivity $\zeta^{\phi}(\omega)$, obtained by solving the quantum Langevin equations, as a function of the homodyne detection angle ϕ. The figures consider the optimal spectrum and sensitivity for both unsqueezed and squeezed input light and for cases where atomic collisions are considered or neglected. Figures 10(a)–10(d) show the variation of $S^{\phi}(\omega)$ and $\zeta^{\phi}(\omega)$ with the detection angle ϕ for models with no collision, as compared to Figs. 10(e)–10(h), where collision or interatomic interactions are considered. From the numerical observations, it is evident that the dominant effect of collision is to shift the spectral peaks, which also causes the sensitivity to shift. This is true for both unsqueezed and squeezed light. Figures 10(a) and 10(c) look at the output spectrum and sensitivity for unsqueezed light, respectively. The maximum of the spectrum occurs at $\phi/\pi = 1/2$, which corresponds to the analytical obtained value. The sensitivity also is best close to the spectral peaks. However, as observed in Figs. 10(b) and 10(d), the variation of S^{ϕ} is no longer straightforward and the maximal value occurs at a different detection angle ϕ. The sensitivity again is optimal close to the spectral peaks.

The variation of the enhancement factor with respect to the homodyne detection angle ϕ and squeezing angle θ, for different squeezing amplitudes r, is shown in Fig. 11. The enhancement factor increases with r, and by adjusting the detection angle the optimal sensitivity can be increased by a factor of 2.5. This is achieved for squeezing amplitude $r = 2$ and the squeezing and detection angles $(\theta, \phi) \in \{(2\pi/3, 2\pi/3), (4\pi/3, \pi/3)\}$.

APPENDIX D: BAE STEADY STATE BEYOND THE RWA

The typical approach to solving the equations of motion in the backaction evasion method is to find solutions in the good cavity regime $\omega_m, G \gg \kappa$, as discussed, for instance, in Ref. [47]. However, steady states of the Hamiltonian can also be obtained in the bad cavity regime, i.e., in the regime $\omega_m, G \ll \kappa$ and $\kappa \gg \Omega \gg \gamma$, under suitable circumstances. The Hamiltonian in Eq. (17) can be written in the interaction picture by transformation with $U = e^{-i[\omega_a a^\dagger a + \omega_m (c^\dagger c + d^\dagger d)]t}$ such that

$$H'/\hbar = \Omega(c^\dagger c - d^\dagger d) + \frac{G}{\sqrt{2}}(c e^{-i\omega_m t} + c^\dagger e^{i\omega_m t} + d e^{-i\omega_m t} + d^\dagger e^{i\omega_m t}) a^\dagger a + (a\varepsilon_+^* e^{i(\delta-\omega_m)t} + a\varepsilon_-^* e^{-i(\delta-\omega_m)t} + \text{H.c.}). \tag{D1}$$

Now the Floquet expansion to the optical operator a is given by $a = \sum_{j=-\infty}^{\infty} a_j e^{ij\delta t}$. Deriving the equation of motion for the expectation value of a and using a mean-field or semiclassical approximation for correlations, the equations are

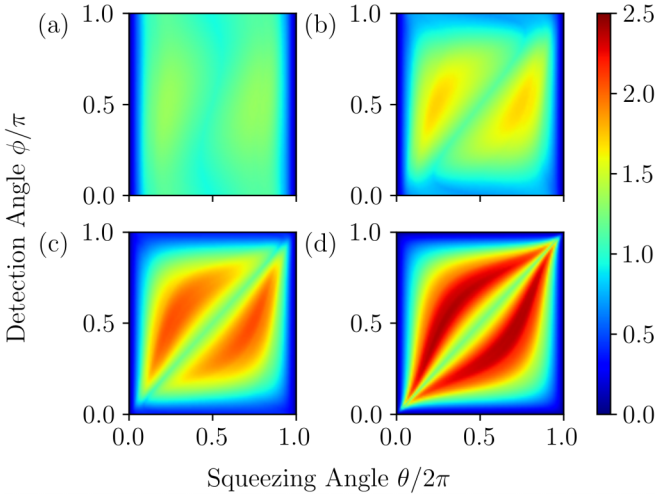

FIG. 11. Variation of sensitivity enhancement factor with detection angle ϕ and squeezing angle θ for different values of squeezing amplitude: (a) $r = 0.1$, (b) $r = 0.5$, (c) $r = 1.0$, and (d) $r = 2.0$.

given by

$$\dot{a} = \sum_{j=-\infty}^{\infty} (ija_j + \dot{a}_j)e^{ij\delta t} \tag{D2}$$

$$= -i\frac{G}{\sqrt{2}}(ce^{-i\omega_m t} + c^\dagger e^{i\omega_m t} + de^{-i\omega_m t} + d^\dagger e^{i\omega_m t})a + \varepsilon_+ - \frac{\kappa}{2}a. \tag{D3}$$

Comparing Eqs. (D2) and (D3), comparing coefficients of $e^{i\delta t}$ up to the first order, and neglecting fluctuations, the relevant relations are

$$\dot{a}_0 = -i\frac{G}{2}(ca_1 + c^\dagger a_{-1} + da_1 + d^\dagger a_{-1}) - \frac{\kappa}{2} \quad \text{(for 0)}, \tag{D4}$$

$$i\delta a_1 + \dot{a}_1 = -i\frac{G}{2}[(c+d)a_2 + (c^\dagger + d^\dagger)a_0] + \varepsilon_+ - \frac{\kappa}{2}a_1 \quad (\text{for } e^{i\delta t}), \tag{D5}$$

$$-i\delta a_{-1} + \dot{a}_{-1} = -i\frac{G}{2}[(c+d)a_0 + (c^\dagger + d^\dagger)a_{-2}] + \varepsilon_- - \frac{\kappa}{2}a_{-1} \quad (\text{for } e^{-i\delta t}). \tag{D6}$$

The second-order terms are

$$2i\delta a_2 + \dot{a}_2 = -i\frac{G}{\sqrt{2}}(c^\dagger + d^\dagger)a_1 - \kappa a_2 \quad (\text{for } e^{2i\delta t}), \tag{D7}$$

$$-2i\delta a_{-2} + \dot{a}_{-2} = -i\frac{G}{\sqrt{2}}(c+d)a_{-1} - \kappa a_{-2} \quad (\text{for } e^{-2i\delta t}). \tag{D8}$$

Assuming that the optical field is stationary and therefore setting all $\dot{a}_j = 0$, the expressions for the steady state are obtained,

$$\bar{a}_2 = \frac{iG\langle c^\dagger + d^\dagger\rangle\bar{a}_1}{\kappa/2 - 2i\delta}, \quad \bar{a}_{-2} = \frac{iG\langle c+d\rangle\bar{a}_{-1}}{\kappa/2 + 2i\delta}, \tag{D9}$$

$$\bar{a}_1 = \frac{\varepsilon_+ - iG(\langle c^\dagger + d^\dagger\rangle\bar{a}_0 + \langle c+d\rangle\bar{a}_2)}{\kappa/2 + i\delta}, \tag{D10}$$

$$\bar{a}_{-1} = \frac{\varepsilon_- - iG(\langle c^\dagger + d^\dagger\rangle\bar{a}_{-2} + \langle c+d\rangle\bar{a}_0)}{\kappa/2 - i\delta}, \tag{D11}$$

$$\bar{a}_0 = -\frac{i\sqrt{2}G(\langle c+d\rangle\bar{a}_1 + \langle c^\dagger + d^\dagger\rangle\bar{a}_{-1})}{\kappa}. \tag{D12}$$

In the bad cavity regime $G, \omega_m \ll \kappa$, the steady-state values of $\bar{a}_{\pm 2}$ are directly proportional to the factor G/κ, which can be significantly small. Therefore, the terms $\bar{a}_{\pm 2}$ and higher orders can be neglected in this regime, and a much simpler solution can be achieved by assuming just the first-order driving amplitudes and atomic sideband modes such that

$$\bar{X}_{c\,(d)} = \bar{X}^{(1)}_{c\,(d)}e^{i\delta t} + \bar{X}^{(-1)}_{c\,(d)}e^{-i\delta t} + \bar{X}^{(0)}_{c\,(d)}. \tag{D13}$$

Substituting the above first-order expanded operators $\bar{X}_{c\,(d)}$ in Eqs. (D6)–(D8) and comparing the different orders, the relations are

$$\bar{a}_0 = 0, \quad \bar{X}^{(\pm 1)}_{c\,(d)} = 0, \tag{D14}$$

$$\bar{X}^{(0)}_{c\,(d)} = -\frac{G}{(\omega_m \pm \Omega)}(|a_0|^2 + |a_1|^2 + |a_{-1}|^2), \tag{D15}$$

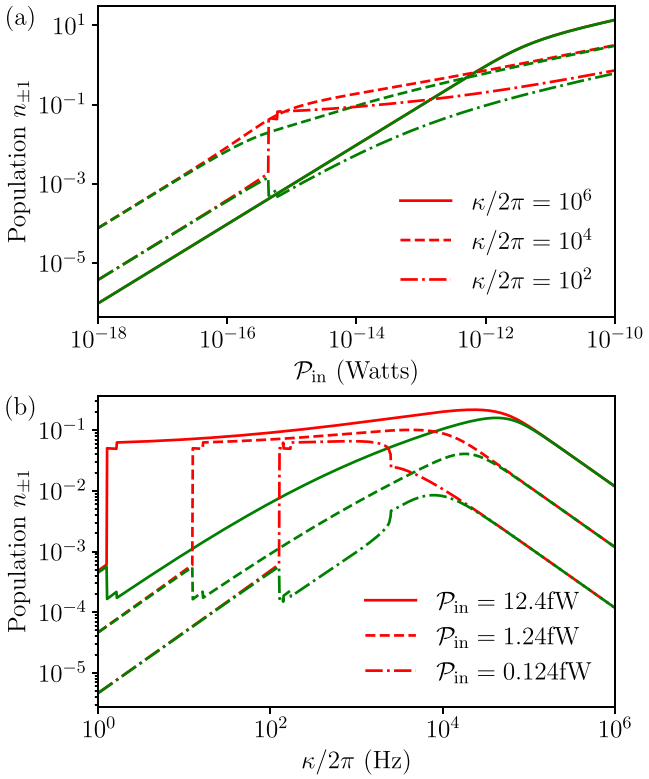

FIG. 12. Optical bistability in the steady-state solutions of the equation of motion in the BAE scheme, as a function of (a) input power $\mathcal{P}_{\rm in}$ and (b) cavity loss rate κ.

$$i\delta\bar{a}_1 = -\frac{\kappa}{2}\bar{a}_1 + i\Omega_{\rm eff}(|a_1|^2 + |a_{-1}|^2)\bar{a}_1 - i\varepsilon_+, \tag{D16}$$

$$i\delta\bar{a}_{-1} = -\frac{\kappa}{2}\bar{a}_{-1} + i\Omega_{\rm eff}(|a_1|^2 + |a_{-1}|^2)\bar{a}_{-1} - i\varepsilon_-, \tag{D17}$$

$$\Omega_{\rm eff} = \frac{G(\Omega_d^2 + \Omega_c^2)}{\Omega_c^2\Omega_d^2 + \mathcal{A}^2} \text{ or } \Omega_{\rm eff} = \frac{2G\omega_m}{\omega_m^2 - \Omega^2}, \tag{D18}$$

where the two values of $\Omega_{\rm eff}$ are for the cases with and without interatomic interaction or collisions in the dynamics, respectively. Making the above substitutions, the steady-state

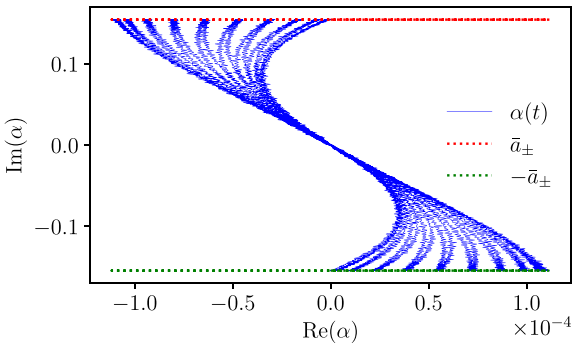

FIG. 13. Phase-space evolution of the coherent-state complex amplitude $\alpha(t)$, obtained numerically. The amplitude is constrained by the analytical bounds obtained by solving for the steady-state equations.

populations $n_{\pm 1} = |\bar{a}_{\pm 1}|^2$ under the above approximations can be solved using a set of coupled cubic equations

$$n_1\left[\left(n_1 + n_{-1} - \frac{\delta}{\Omega_{\text{eff}}}\right)^2 + \left(\frac{\kappa}{\Omega_{\text{eff}}}\right)^2\right] = \frac{|\varepsilon_+|^2}{\Omega_{\text{eff}}^2},$$
$$n_{-1}\left[\left(n_1 + n_{-1} + \frac{\delta}{\Omega_{\text{eff}}}\right)^2 + \left(\frac{\kappa}{\Omega_{\text{eff}}}\right)^2\right] = \frac{|\varepsilon_-|^2}{\Omega_{\text{eff}}^2}. \quad \text{(D19)}$$

Note that the occupation numbers of the two steady states can be different, i.e., $n_1 \neq n_{-1}$.

The linearization of the equation of motion is based on the assumption that the operators can be written as the sum of a steady state and fluctuations. As such, it is necessary that a monostable steady state exists in the regime $G \ll \kappa$. Solving Eq. (D19) numerically exhibits the region of bistability that appears as a sharp discontinuity in the sideband populations $n_\pm$ as the input power or the cavity dissipation rate is varied as shown in Fig. 12. For lower input power $\mathcal{P}_{\text{in}}$, a monostable region exists for most cavity dissipation. For higher input powers, to avoid bistability, it is sufficient to choose the cavity dissipation rate $\kappa/2\pi \geqslant 10^5$ Hz.

If the term G is very small, the second terms on the right-hand sides of Eqs. (D16) and (D17) vanish and the steady-state solution reduces to $\bar{a} = a_s = \frac{|\varepsilon_\pm|}{\delta^2 + (\kappa/2)^2}$. This can then be considered to be the steady-state value to linearize the optical operators in the BAE scheme. The validity of the above analytical expression can be checked by numerically solving the time-dependent set of differential equations in the mean-field regime obtained from Eq. (D1). The time-dependent complex solution α of the optical field is bounded in the phase space under the steady-state oscillation amplitude $|\bar{a}_\pm|$, as shown in Fig. 13. This shows that the solutions of the differential equations in the phase space are strictly bounded by the steady-state amplitudes, which can then be used to find the operable monostable regions where rotational sensitivity is to be measured.

APPENDIX E: SPECTRAL DENSITY COEFFICIENTS FOR THE BAE SCHEME

The coefficients $\{A(\omega), B(\omega), C(\omega), D(\omega)\}$ in the expressions for the optical quadrature and the spectral density components in Eqs. (36)–(39), respectively, are obtained from the solutions in Eqs. (30)–(35). These coefficients, with respect to the output optical quadrature $P_{\text{out}}(\omega)$, are

$$A^0(\omega) = \sqrt{2}\kappa\chi_a^2(\omega)\bar{a}_\pm^2[\chi_c(\omega-\delta) + \chi_c(\omega+\delta) + \chi_d(\omega-\delta) + \chi_d(\omega+\delta)], \quad \text{(E1)}$$

$$B^0(\omega) = -\kappa\chi_a(\omega) - 1, \quad \text{(E2)}$$

$$C^{\pm 1}(\omega) = \sqrt{2\kappa}G\bar{a}\chi_a(\omega \pm \delta)(\omega_m + \Omega)\chi_c(\omega), \quad \text{(E3)}$$

$$D^{\pm 1}(\omega) = \sqrt{2\kappa}G\bar{a}\chi_a(\omega \pm \delta)(\omega_m - \Omega)\chi_d(\omega), \quad \text{(E4)}$$

$$A^{\pm 2}(\omega) = \sqrt{2}\kappa G^2\bar{a}^2\chi_a(\omega \mp 2\delta)\chi_a(\omega)[\chi_c(\omega \mp \delta) + \chi_d(\omega \mp \delta)], \quad \text{(E5)}$$

where all higher-order coefficients are zero, which truncates the Floquet expansion at the second order.

[1] M. Lewenstein, A. Sanpera, V. Ahufinger, B. Damski, A. Sen(De), and U. Sen, Ultracold atomic gases in optical lattices: Mimicking condensed matter physics and beyond, Adv. Phys. **56**, 243 (2007).

[2] I. Bloch, J. Dalibard, and W. Zwerger, Many-body physics with ultracold gases, Rev. Mod. Phys. **80**, 885 (2008).

[3] G. Barontini and S. Worm, Measuring the stability of fundamental constants with a network of clocks, EPJ Quantum Technol. **9**, 12 (2022).

[4] S. O. Allehabi, V. A. Dzuba, and V. V. Flambaum, Atomic clocks highly sensitive to the variation of the fine-structure constant based on Hf II, Hf IV, and W VI ions, Phys. Rev. A **106**, 032807 (2022).

[5] G. K. Campbell and W. D. Phillips, Ultracold atoms and precise time standards, Philos. Trans. R. Soc. A **369**, 4078 (2011).

[6] Boulder Atomic Clock Optical Network (BACON) Collaboration, Frequency ratio measurements at 18-digit accuracy using an optical clock network, Nature (London) **591**, 564 (2021).

[7] G. E. Marti, R. Olf, and D. M. Stamper-Kurn, Collective excitation interferometry with a toroidal Bose-Einstein condensate, Phys. Rev. A **91**, 013602 (2015).

[8] S. Ragole and J. M. Taylor, Interacting atomic interferometry for rotation sensing approaching the Heisenberg limit, Phys. Rev. Lett. **117**, 203002 (2016).

[9] G. Pelegrí, J. Mompart, and V. Ahufinger, Quantum sensing using imbalanced counter-rotating Bose–Einstein condensate modes, New J. Phys. **20**, 103001 (2018).

[10] C. Ryu, M. F. Andersen, P. Cladé, V. Natarajan, K. Helmerson, and W. D. Phillips, Observation of persistent flow of a Bose-Einstein condensate in a toroidal trap, Phys. Rev. Lett. **99**, 260401 (2007).

[11] B. E. Sherlock, M. Gildemeister, E. Owen, E. Nugent, and C. J. Foot, Time-averaged adiabatic ring potential for ultracold atoms, Phys. Rev. A **83**, 043408 (2011).

[12] C. Ryu, P. W. Blackburn, A. A. Blinova, and M. G. Boshier, Experimental realization of Josephson junctions for an atom SQUID, Phys. Rev. Lett. **111**, 205301 (2013).

[13] S. Beattie, S. Moulder, R. J. Fletcher, and Z. Hadzibabic, Persistent currents in spinor condensates, Phys. Rev. Lett. **110**, 025301 (2013).

[14] F. Brennecke, S. Ritter, T. Donner, and T. Esslinger, Cavity optomechanics with a Bose-Einstein condensate, Science **322**, 235 (2008).

[15] S. Ritter, F. Brennecke, K. Baumann, T. Donner, C. Guerlin, and T. Esslinger, Dynamical coupling between a Bose–Einstein condensate and a cavity optical lattice, Appl. Phys. B **95**, 213 (2009).

[16] K. Baumann, C. Guerlin, F. Brennecke, and T. Esslinger, Dicke quantum phase transition with a superfluid gas in an optical cavity, Nature (London) **464**, 1301 (2010).

[17] K. C. Wright, R. B. Blakestad, C. J. Lobb, W. D. Phillips, and G. K. Campbell, Driving phase slips in a superfluid atom circuit with a rotating weak link, Phys. Rev. Lett. **110**, 025302 (2013).

[18] K. Snizhko, K. Isaieva, Y. Kuriatnikov, Y. Bidasyuk, S. Vilchinskii, and A. Yakimenko, Stochastic phase slips in toroidal Bose-Einstein condensates, Phys. Rev. A **94**, 063642 (2016).

[19] A. Ramanathan, K. C. Wright, S. R. Muniz, M. Zelan, W. T. Hill, C. J. Lobb, K. Helmerson, W. D. Phillips, and G. K. Campbell, Superflow in a toroidal Bose-Einstein condensate: An atom circuit with a tunable weak link, Phys. Rev. Lett. **106**, 130401 (2011).

[20] L. Amico, D. Anderson, M. Boshier, J.-P. Brantut, L.-C. Kwek, A. Minguzzi, and W. von Klitzing, *Colloquium*: Atomtronic circuits: From many-body physics to quantum technologies, Rev. Mod. Phys. **94**, 041001 (2022).

[21] S. R. Muniz, D. S. Naik, and C. Raman, Bragg spectroscopy of vortex lattices in Bose-Einstein condensates, Phys. Rev. A **73**, 041605(R) (2006).

[22] B. Mukherjee, A. Shaffer, P. B. Patel, Z. Yan, C. C. Wilson, V. Crépel, R. J. Fletcher, and M. Zwierlein, Crystallization of bosonic quantum Hall states in a rotating quantum gas, Nature (London) **601**, 58 (2022).

[23] B. P. Anderson, P. C. Haljan, C. E. Wieman, and E. A. Cornell, Vortex precession in Bose-Einstein condensates: Observations with filled and empty cores, Phys. Rev. Lett. **85**, 2857 (2000).

[24] A. Kumar, N. Anderson, W. D. Phillips, S. Eckel, G. K. Campbell, and S. Stringari, Minimally destructive, Doppler measurement of a quantized flow in a ring-shaped Bose–Einstein condensate, New J. Phys. **18**, 025001 (2016).

[25] S. Safaei, L.-C. Kwek, R. Dumke, and L. Amico, Monitoring currents in cold-atom circuis, Phys. Rev. A **100**, 013621 (2019).

[26] P. Kumar, T. Biswas, K. Feliz, R. Kanamoto, M.-S. Chang, A. K. Jha, and M. Bhattacharya, Cavity optomechanical sensing and manipulation of an atomic persistent current, Phys. Rev. Lett. **127**, 113601 (2021).

[27] N. Pradhan, P. Kumar, R. Kanamoto, T. N. Dey, M. Bhattacharya, and P. K. Mishra, Cavity optomechanical detection of persistent currents and solitons in a bosonic ring condensate, Phys. Rev. Res. **6**, 013104 (2024).

[28] N. Pradhan, P. Kumar, R. Kanamoto, T. N. Dey, M. Bhattacharya, and P. K. Mishra, Ring Bose-Einstein condensate in a cavity: Chirality detection and rotation sensing, Phys. Rev. A **109**, 023524 (2024).

[29] M. Aspelmeyer, T. J. Kippenberg, and F. Marquardt, Cavity optomechanics, Rev. Mod. Phys. **86**, 1391 (2014).

[30] L. Allen, S. Barnett, and M. Padgett, *Optical Angular Momentum* (IOP, Bristol, 2003).

[31] P. H. Kim, B. D. Hauer, C. Doolin, F. Souris, and J. P. Davis, Approaching the standard quantum limit of mechanical torque sensing, Nat. Commun. **7**, 13165 (2016).

[32] C. M. Caves, Quantum-mechanical radiation-pressure fluctuations in an interferometer, Phys. Rev. Lett. **45**, 75 (1980).

[33] K. Børkje, A. Nunnenkamp, B. M. Zwickl, C. Yang, J. G. E. Harris, and S. M. Girvin, Observability of radiation-pressure shot noise in optomechanical systems, Phys. Rev. A **82**, 013818 (2010).

[34] T. P. Purdy, R. W. Peterson, and C. A. Regal, Observation of radiation pressure shot noise on a macroscopic object, Science **339**, 801 (2013).

[35] C. M. Caves, Quantum-mechanical noise in an interferometer, Phys. Rev. D **23**, 1693 (1981).

[36] C. Fabre, M. Pinard, S. Bourzeix, A. Heidmann, E. Giacobino, and S. Reynaud, Quantum-noise reduction using a cavity with a movable mirror, Phys. Rev. A **49**, 1337 (1994).

[37] K. S. Thorne, R. W. P. Drever, C. M. Caves, M. Zimmermann, and V. D. Sandberg, Quantum nondemolition measurements of harmonic oscillators, Phys. Rev. Lett. **40**, 667 (1978).

[38] V. B. Braginsky, Y. I. Vorontsov, and K. S. Thorne, Quantum nondemolition measurements, Science **209**, 547 (1980).

[39] H. J. Kimble, Y. Levin, A. B. Matsko, K. S. Thorne, and S. P. Vyatchanin, Conversion of conventional gravitational-wave interferometers into quantum nondemolition interferometers by modifying their input and/or output optics, Phys. Rev. D **65**, 022002 (2001).

[40] T. P. Purdy, P.-L. Yu, R. W. Peterson, N. S. Kampel, and C. A. Regal, Strong optomechanical squeezing of light, Phys. Rev. X **3**, 031012 (2013).

[41] N. S. Kampel, R. W. Peterson, R. Fischer, P.-L. Yu, K. Cicak, R. W. Simmonds, K. W. Lehnert, and C. A. Regal, Improving broadband displacement detection with quantum correlations, Phys. Rev. X **7**, 021008 (2017).

[42] C. B. Møller, R. A. Thomas, G. Vasilakis, E. Zeuthen, Y. Tsaturyan, M. Balabas, K. Jensen, A. Schliesser, K. Hammerer, and E. S. Polzik, Quantum back-action-evading measurement of motion in a negative mass reference frame, Nature (London) **547**, 191 (2017).

[43] I. Shomroni, L. Qiu, D. Malz, A. Nunnenkamp, and T. J. Kippenberg, Optical backaction-evading measurement of a mechanical oscillator, Nat. Commun. **10**, 2086 (2019).

[44] D. Ganapathy *et al.* (LIGO O4 Detector Collaboration), Broadband quantum enhancement of the LIGO detectors with frequency-dependent squeezing, Phys. Rev. X **13**, 041021 (2023).

[45] V. B. Braginsky, F. Y. Khalili, and K. S. Thorne, *Quantum Measurement* (Cambridge University Press, Cambridge, 1992).

[46] A. A. Clerk, M. H. Devoret, S. M. Girvin, F. Marquardt, and R. J. Schoelkopf, Introduction to quantum noise, measurement, and amplification, Rev. Mod. Phys. **82**, 1155 (2010).

[47] M. J. Woolley and A. A. Clerk, Two-mode back-action-evading measurements in cavity optomechanics, Phys. Rev. A **87**, 063846 (2013).

[48] D. Malz and A. Nunnenkamp, Floquet approach to bichromatically driven cavity-optomechanical systems, Phys. Rev. A **94**, 023803 (2016).

[49] D. Malz and A. Nunnenkamp, Optomechanical dual-beam backaction-evading measurement beyond the rotating-wave approximation, Phys. Rev. A **94**, 053820 (2016).

[50] M. Brunelli, D. Malz, and A. Nunnenkamp, Conditional dynamics of optomechanical two-tone backaction-evading measurements, Phys. Rev. Lett. **123**, 093602 (2019).

[51] S. Ghosh, M. A. Feldman, S. Hong, C. Marvinney, R. Pooser, and J. M. Taylor, Combining quantum noise reduction resources: A practical approach, arXiv:2211.14460.

[52] O. Morizot, Y. Colombe, V. Lorent, H. Perrin, and B. M. Garraway, Ring trap for ultracold atoms, Phys. Rev. A **74**, 023617 (2006).

[53] D. Naidoo, K. Aït-Ameur, M. Brunel, and A. Forbes, Intracavity generation of superpositions of Laguerre–Gaussian beams, Appl. Phys. B **106**, 683 (2012).

[54] P. B. Blakie and R. J. Ballagh, Spatially selective Bragg scattering: A signature for vortices in Bose-Einstein condensates, Phys. Rev. Lett. **86**, 3930 (2001).

[55] T. Langen, M. Gring, M. Kuhnert, B. Rauer, R. Geiger, D. A. Smith, I. E. Mazets, and J. Schmiedmayer, Prethermalization in one-dimensional Bose gases: Description by a stochastic Ornstein-Uhlenbeck process, Eur. Phys. J.: Spec. Top. **217**, 43 (2013).

[56] A. Barchielli and B. Vacchini, Quantum Langevin equations for optomechanical systems, New J. Phys. **17**, 083004 (2015).

[57] L.-A. Wu, M. Xiao, and H. J. Kimble, Squeezed states of light from an optical parametric oscillator, J. Opt. Soc. Am. B **4**, 1465 (1987).

[58] T. Park, H. Stokowski, V. Ansari, S. Gyger, K. K. S. Multani, O. T. Celik, A. Y. Hwang, D. J. Dean, F. Mayor, T. P. McKenna, M. M. Fejer, and A. Safavi-Naeini, Single-mode squeezed-light generation and tomography with an integrated optical parametric oscillator, Sci. Adv. **10**, eadl1814 (2024).

[59] C. W. Gardiner and P. Zoller, *Quantum Noise: A Handbook of Markovian and Non-Markovian Quantum Stochastic Methods with Applications to Quantum Optics*, Springer Series in Synergetics (Springer, Berlin, 2004).

[60] R. S. Schoenfeld and W. Harneit, Real time magnetic field sensing and imaging using a single spin in diamond, Phys. Rev. Lett. **106**, 030802 (2011).

[61] C. M. Caves, K. S. Thorne, R. W. P. Drever, V. D. Sandberg, and M. Zimmermann, On the measurement of a weak classical force coupled to a quantum-mechanical oscillator. I. Issues of principle, Rev. Mod. Phys. **52**, 341 (1980).

[62] M. F. Bocko and R. Onofrio, On the measurement of a weak classical force coupled to a harmonic oscillator: Experimental progress, Rev. Mod. Phys. **68**, 755 (1996).

[63] P. Grangier, J. A. Levenson, and J.-P. Poizat, Quantum non-demolition measurements in optics, Nature (London) **396**, 537 (1998).

[64] A. A. Clerk, F. Marquardt, and K. Jacobs, Back-action evasion and squeezing of a mechanical resonator using a cavity detector, New J. Phys. **10**, 095010 (2008).

[65] M. Tsang and C. M. Caves, Coherent quantum-noise cancellation for optomechanical sensors, Phys. Rev. Lett. **105**, 123601 (2010).

[66] M. Tsang and C. M. Caves, Evading quantum mechanics: Engineering a classical subsystem within a quantum environment, Phys. Rev. X **2**, 031016 (2012).

[67] J. Stenger, S. Inouye, A. P. Chikkatur, D. M. Stamper-Kurn, D. E. Pritchard, and W. Ketterle, Bragg spectroscopy of a Bose-Einstein condensate, Phys. Rev. Lett. **82**, 4569 (1999).